14. Gregorio F, Cristallini S, Santeusanio F, Filipponi P, Fumelli P (1994) Osteopenia associated with non-insulin-dependent diabetes mellitus: what are the causes? Diabetes Res Clin Pract 23:43–54
CrossRef ChemPort PubMed

15. Levin ME, Boisseau VC, Avioli LV (1976) Effects of diabetes mellitus on bone mass in juvenile and adult-onset diabetes. N Engl J Med 294:241–245
ChemPort PubMed

16. Haffner SM, Bauer RL (1993) The association of obesity and glucose and insulin concentrations with bone density in premenopausal and postmenopausal women. Metabolism 42:735–738
CrossRef ChemPort PubMed

17. Reid IR, Evans MC, Cooper GJ, Ames RW, Stapleton J (1993) Circulating insulin levels are related to bone density in normal postmenopausal women. Am J Physiol 265:E655–659
ChemPort PubMed

18. Stolk RP, van Daele PL, Pols HA, Burger H, Hofman A, Birkenhager JC, Lamberts SW, Grobbee DE (1996) Hyperinsulinemia and bone mineral density in an elderly population: The Rotterdam Study. Bone 18:545–549
CrossRef ChemPort PubMed

19. Barrett-Connor E, Kritz-Silverstein D (1996) Does hyperinsulinemia preserve bone? Diabetes Care 19:1388–1392
ChemPort PubMed

20. Akanuma Y (1996) Non-insulin-dependent diabetes mellitus (NIDDM) in Japan. Diabet Med 13:S11–S12
ChemPort

21. Yoshinaga H, Kosaka K (1999) Heterogeneous relationship of early insulin response and fasting insulin level with development of non-insulin-dependent diabetes mellitus in non-diabetic Japanese subjects with or without obesity. Diabetes Res Clin Pract 44:129–136
CrossRef ChemPort PubMed

22. Leite Duarte ME, da Silva RD (1996) Histomorphometric analysis of the bone tissue in patients with non-insulin-dependent diabetes (DMNID). Rev Hosp Clin Fac Med Sao Paulo 51:7–11
PubMed

23. Yano H, Ohya K, Amagasa T (1996) Insulin enhancement of in vitro wound healing in fetal rat parietal bones. J Oral Maxillofac Surg 54:182–186
CrossRef ChemPort PubMed

24. Cornish J, Callon KE, Cooper GJ, Reid IR (1995) Amylin stimulates osteoblast proliferation and increases mineralized bone volume in adult mice. Biochem Biophys Res Commun 207:133–139
CrossRef ChemPort PubMed

25. Mitsukawa T, Takemura J, Asai J, Nakazato M, Kangawa K, Matsuo H, Matsukura S (1990) Islet amyloid polypeptide response to glucose, insulin, and somatostatin analogue administration. Diabetes 39:639–642
ChemPort PubMed

26. Hartter E, Svoboda T, Ludvik B, Schuller M, Lell B, Kuenburg E, Brunnbauer M, Woloszczuk W, Prager R (1991) Basal and stimulated plasma levels of pancreatic amylin indicate its co-secretion with insulin in humans. Diabetologia 34:52–54
ChemPort PubMed

27. Khaw KT, Barrett-Connor E (1991) Fasting plasma glucose levels and endogenous androgens in non-diabetic postmenopausal women. Clin Sci (Lond) 80:199–203

28. Riis BJ, Overgaard K, Christiansen C (1995) Biochemical markers of bone turnover to monitor the bone response to postmenopausal hormone replacement therapy. Osteoporos Int 5:276–280
ChemPort PubMed

29. Anderson FH, Francis RM, Faulkner K (1996) Androgen supplementation in eugonadal men with osteoporosis—effects of 6 months of treatment on bone mineral density and cardiovascular risk factors. Bone 18:171–177
CrossRef ChemPort PubMed

30. Nestler JE (1993) Sex hormone-binding globulin: a marker for hyperinsulinemia and/or insulin resistance? J Clin Endocrinol Metab 76:273–274
CrossRef ChemPort PubMed

31. van Hemert AM, Birkenhager JC, De Jong FH, Vandenbroucke JP, Valkenburg HA (1989) Sex hormone binding globulin in postmenopausal women: a predictor of osteoporosis superior to endogenous oestrogens. Clin Endocrinol (Oxf) 31:499–509

32. Balint E, Szabo P, Marshall CF, Sprague SM (2001) Glucose-induced inhibition of in vitro bone mineralization. Bone 28:21–28
CrossRef ChemPort PubMed

33. Williams JP, Blair HC, McDonald JM, McKenna MA, Jordan SE, Williford J, Hardy RW (1997) Regulation of osteoclastic bone resorption by glucose. Biochem Biophys Res Commun 235:646–651
CrossRef ChemPort PubMed

34. Nagasaka S, Murakami T, Uchikawa T, Ishikawa SE, Saito T (1995) Effect of glycemic control on calcium and phosphorus handling and parathyroid hormone level in patients with non-insulin-dependent diabetes mellitus. Endocr J 42:377–383
ChemPort PubMed

35. Okazaki R, Totsuka Y, Hamano K, Ajima M, Miura M, Hirota Y, Hata K, Fukumoto S, Matsumoto T (1997) Metabolic improvement of poorly controlled noninsulin-dependent diabetes mellitus decreases bone turnover. J Clin Endocrinol Metab 82:2915–2920
CrossRef ChemPort PubMed

36. Stepan J, Havranek T, Formankova J, Skrha J, Skrha F, Pacovsky V (1980) Bone isoenzyme of serum alkaline phosphatase in diabetes mellitus. Clin Chim Acta 105:75–81
CrossRef ChemPort PubMed

37. Stein GS, Lian JB (1993) Molecular mechanisms mediating proliferation/differentiation interrelationships during progressive development of the osteoblast phenotype. Endocr Rev 14:424–442
CrossRef ChemPort PubMed

nature medicine

Overexpression of CNP in chondrocytes rescues achondroplasia through a MAPK-dependent pathway

Akihiro Yasoda[1], Yasato Komatsu[1], Hideki Chusho[1], Takashi Miyazawa[1], Ami Ozasa[1], Masako Miura[1], Tatsuya Kurihara[2], Tomohiro Rogi[2], Shoji Tanaka[2], Michio Suda[1], Naohisa Tamura[1], Yoshihiro Ogawa[1] & Kazuwa Nakao[1]

Achondroplasia is the most common genetic form of human dwarfism, for which there is presently no effective therapy. C-type natriuretic peptide (CNP) is a newly identified molecule that regulates endochondral bone growth through GC-B, a subtype of particulate guanylyl cyclase. Here we show that targeted overexpression of CNP in chondrocytes counteracts dwarfism in a mouse model of achondroplasia with activated fibroblast growth factor receptor 3 (FGFR-3) in the cartilage. CNP prevented the shortening of achondroplastic bones by correcting the decreased extracellular matrix synthesis in the growth plate through inhibition of the MAPK pathway of FGF signaling. CNP had no effect on the STAT-1 pathway of FGF signaling that mediates the decreased proliferation and the delayed differentiation of achondroplastic chondrocytes. These results demonstrate that activation of the CNP–GC-B system in endochondral bone formation constitutes a new therapeutic strategy for human achondroplasia.

Achondroplasia is the most common genetic form of human dwarfism, with a prevalence at birth of about 1/26,000 (ref. 1). Effective therapy for this condition has not as yet been established. Recent advances in molecular genetics have shown that constitutively active mutations in the gene encoding FGFR-3 are responsible for human achondroplasia[2–4]. Constitutive activation of FGFR-3 stimulates various intracellular signaling pathways, including the MAPK and STAT-1 pathways[5]. It has been reported that the STAT-1 pathway of FGFR-3 signaling inhibits endochondral bone growth[6,7]; the contribution of the MAPK pathway, another major component of FGFR-3 signaling, remains unclear.

The natriuretic peptide family consists of three structurally related peptides: atrial natriuretic peptide (ANP), brain natriuretic peptide (BNP) and CNP[8]. They exert biological actions by accumulation of intracellular cGMP mediated by two subtypes of particulate guanylyl cyclase: guanylyl cyclase-A (GC-A) for ANP and BNP and guanylyl cyclase-B (GC-B) for CNP[9,10]. Although the natriuretic peptide system has mainly been implicated in regulating the cardiovascular system, we have shown that the CNP–GC-B system is an important regulator of endochondral bone growth[11–14]. Activation of the CNP–GC-B system in transgenic mice with elevated plasma concentrations of BNP[11] or in mice depleted of the clearance receptor for natriuretic peptides[15,16] results in very similar skeletal overgrowth. By contrast, inactivation of the CNP–GC-B pathway in mice depleted of CNP[13] or cGMP-dependent protein kinase II[14], a downstream mediator of the CNP–GC-B system, results in dwarfism caused by defects in endochondral ossification.

Growth plates stimulated by the CNP–GC-B system have widened proliferative and hypertrophic chondrocyte layers, much like those in FGFR-3-depleted bones[12,17,18]. CNP depletion, by contrast, leads to impaired bone growth resembling that of achondroplastic bones, with a similar histological picture of decreased width in both the proliferative and hypertrophic chondrocyte layers of the growth plate[13,19]. These observations raise the possibility that the CNP–GC-B system in endochondral ossification reverses the inhibitory effect of the FGFs–FGFR-3 system in skeletogenesis. As for the interaction of these systems, marked elevation of cGMP induced by CNP has been reported to block activation of the MAPK cascade induced by FGFs in fibroblasts[20] and mesangeal cells[21].

Here, we developed transgenic mice (*Nppc* mice) with targeted overexpression of CNP in growth-plate cartilage using a transgene containing *Col2a1*, a cartilage-specific promoter[22], and *Nppc*, the gene encoding CNP. Using a mouse model of achondroplasia with activated FGFR-3 in cartilage (*Fgfr3*^{ach} mice)[19], we generated and analyzed doubly transgenic *Nppc Fgfr3*^{ach} mice that overexpress CNP in achondroplastic growth-plate chondrocytes to assess the growth-promoting effect of the CNP–GC-B system on achondroplastic bones and the molecular mechanisms by which this occurs.

RESULTS

Generation of *Nppc* mice

We obtained two strains of *Nppc*-transgenic founders of similar phenotype, and one of them, carrying ten copies of the transgene (*Col2a1*-

[1]Department of Medicine and Clinical Science, Kyoto University Graduate School of Medicine, 54 Shogoin Kawahara-cho Sakyo-ku, Kyoto 606-8507, Japan. [2]Daiichi Suntory Institute for Biomedical Research, 1-1-1 Wakayamadai, Shimamoto-cho, Mishima-gun, Osaka 618-8503, Japan. Correspondence should be addressed to K.N. (nakao@kuhp.kyoto-u.ac.jp).

Published online 14 December 2003; doi:10.1038/nm971

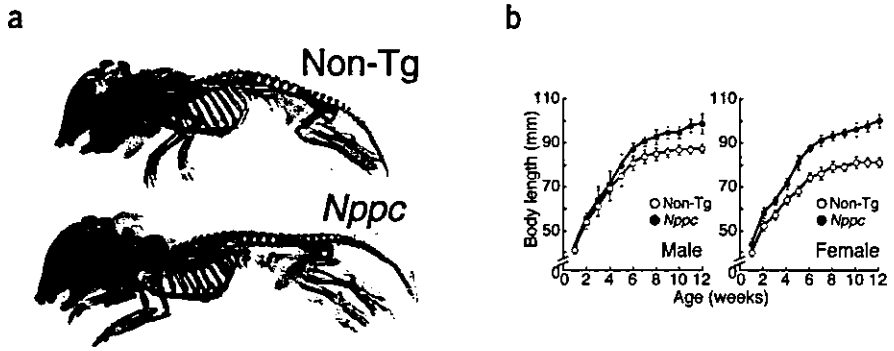

Figure 1 Generation of *Nppc* mice. (**a**) Whole skeletons of nontransgenic (Non-Tg) and *Nppc* mice at birth. (**b**) Growth curves of male (left) and female (right) nontransgenic and *Nppc* mice. (**c**) Bone lengths of 3-month-old female mice. *, $P < 0.05$, $n = 4–5$. (**d**,**e**) Histological analysis of the tibial growth plate of 2-week-old mice. Nontransgenic (left) and *Nppc* (right) in each panel. Alcian blue and H&E staining (**d**) and von Kossa staining (**e**). Arrows indicate growth-plate cartilage in **d**. Scale bar, 200 μm (**d**) or 100 μm (**c**).

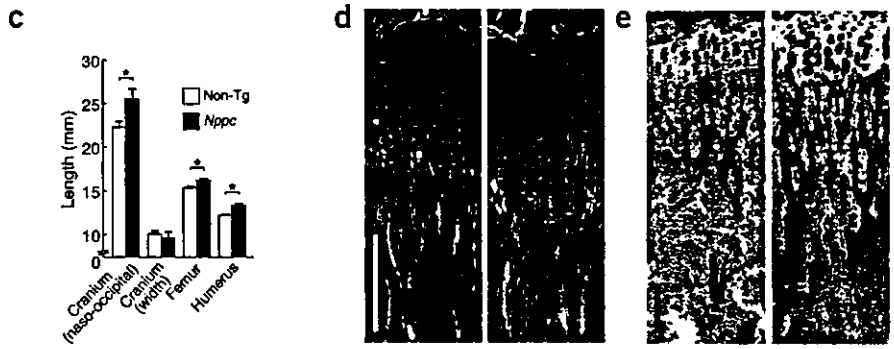

At birth, the whole skeleton of *Nppc* mice showed a substantial longitudinal overgrowth of bones, including long bones of limbs, vertebrae and skull (Fig. 1a). No delay in ossification was observed in the periphery of limbs at this stage. Longitudinal overgrowth of *Nppc* mice became prominent in adulthood. The growth curve shows that the naso-anal lengths of 10-week-old male and female *Nppc* mice were 10% and 19% larger, respectively, than those of their nontransgenic littermates (Fig. 1b). The growth-promoting effect in *Nppc* mice was more prominant in females than in males, so we used female mice in later experiments. The length of bones formed through endochondral ossification (cranium, femur and humerus) were significantly larger in *Nppc* mice than in nontransgenic mice, whereas the width of the cranium, which is determined by membranous ossification, did not differ between the two genotypes (Fig. 1c).

Nppc), was used for further analysis. Targeted overexpression of CNP in the cartilage of these *Nppc* mice was confirmed by RT-PCR (see **Supplementary Fig. 1** online). The production of cGMP, the second messenger of CNP, was about nine times higher in the cartilage of *Nppc* mice than in that of their nontransgenic littermates (18.5 ± 1.5 versus 2.1 ± 0.7 fmol/mg protein, $P < 0.01$).

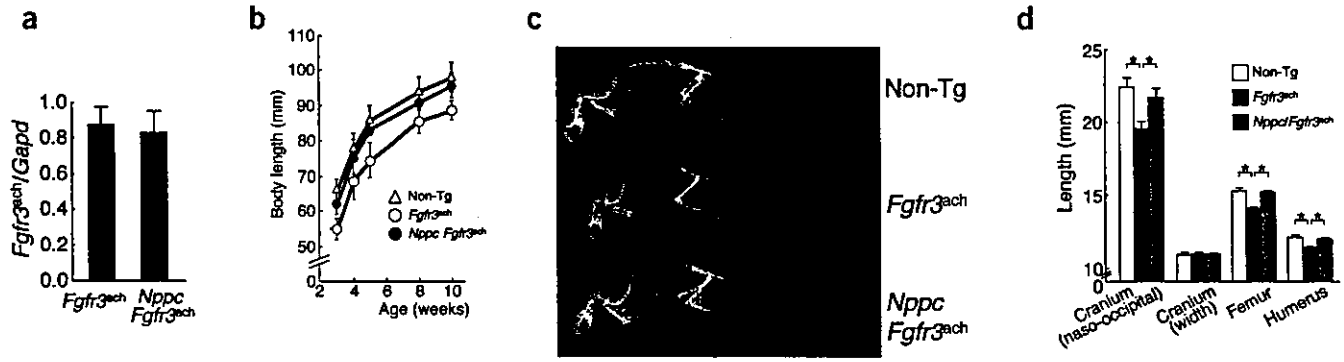

Figure 2 Skeletal rescue of *Fgfr3*^{ach} mice by overexpression of CNP in cartilage. (**a**) Expression of *Fgfr3*^{ach} transgene estimated by quantitative RT-PCR in cartilage of *Fgfr3*^{ach} and *Nppc Fgfr3*^{ach} mice. (**b**) Growth curve of female nontransgenic, *Fgfr3*^{ach} and *Nppc Fgfr3*^{ach} mice. (**c**) Whole skeletons. (**d**) Bone lengths. *, $P < 0.05$, $n = 4–5$. (**e**,**f**) Dose-response effect of CNP on achondroplastic bones. Immunostaining of CNP in neonatal rib cartilage (**e**) and ulnar lengths in 2-month-old female nontransgenic, *Fgfr3*^{ach}, *Nppc*-heterozygous (hetero) *Fgfr3*^{ach} and *Nppc*-homozygous (homo) *Fgfr3*^{ach} mice (**f**). * and ** in **f**, $P < 0.05$ and $P < 0.01$, respectively, $n = 3–5$.

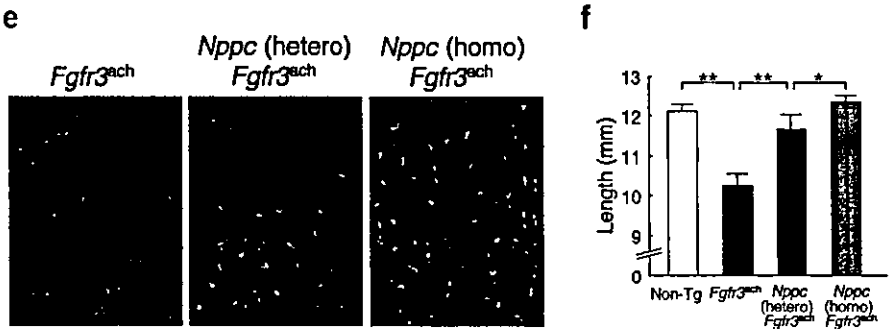

Histological examination showed that *Nppc* mice had wider growth plates than their nontransgenic littermates (Fig. 1d). In the tibiae of 2-week-old mice, the proliferative and hypertrophic chondrocyte layers express type II and X collagens, respectively, as shown by *in situ* hybridization (see Supplementary Fig. 2 online). These layers were significantly wider in *Nppc* mice than in nontransgenic mice (proliferative: 234 ± 12 versus 207 ± 14 μm, $P < 0.05$; hypertrophic: 215 ± 3 versus 193 ± 16 μm, $P < 0.05$). The intensities of *Col2a1* and *Col10a1* mRNA expression did not differ between the two genotypes. Each hypertrophic chondrocyte was enlarged in *Nppc* mice as compared with their nontransgenic littermates (Fig. 1d and Supplementary Fig. 2 online). Von Kossa staining of the proximal tibiae showed that subchondral trabeculae were more abundant and longer in *Nppc* mice than in nontransgenic mice (Fig. 1e). In addition, assessment by peripheral quantitative computed tomography (pQCT) showed that the bone mineral density of trabecular bones in the proximal tibiae of 12-week-old *Nppc* mice is significantly larger than that of their nontransgenic littermates (202.2 ± 6.4 versus 188.3 ± 5.3 g/mm^3, $P < 0.05$).

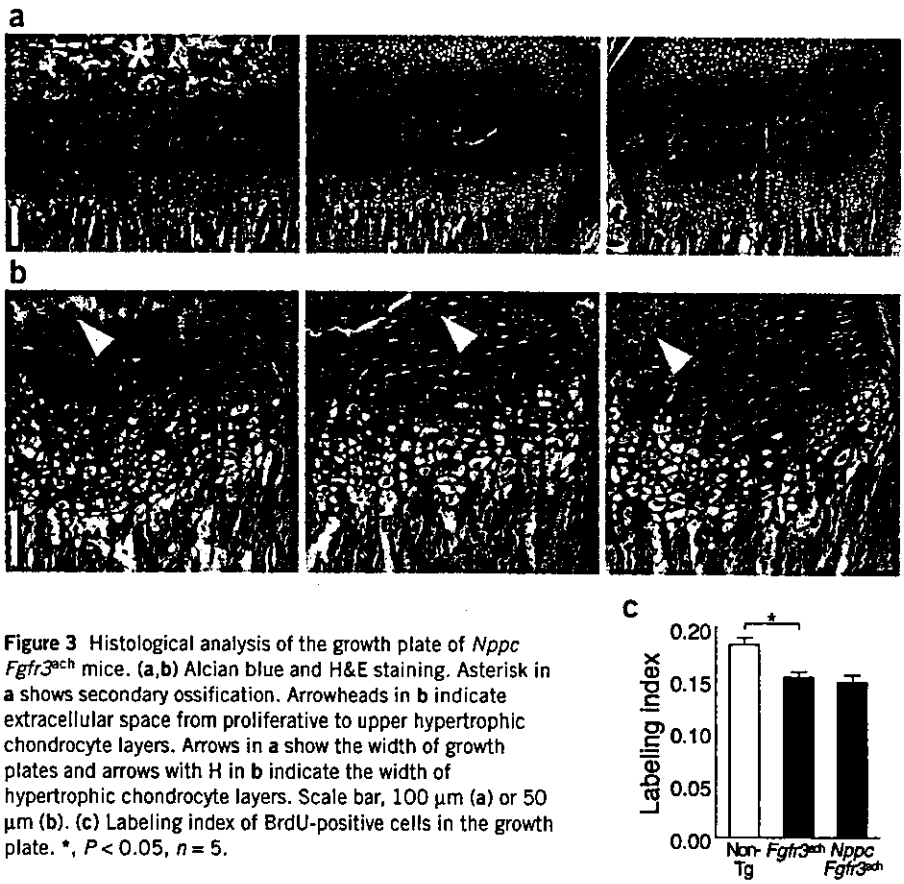

Figure 3 Histological analysis of the growth plate of *Nppc Fgfr3*^{ach} mice. (**a**,**b**) Alcian blue and H&E staining. Asterisk in **a** shows secondary ossification. Arrowheads in **b** indicate extracellular space from proliferative to upper hypertrophic chondrocyte layers. Arrows in **a** show the width of growth plates and arrows with H in **b** indicate the width of hypertrophic chondrocyte layers. Scale bar, 100 μm (**a**) or 50 μm (**b**). (**c**) Labeling index of BrdU-positive cells in the growth plate. *, $P < 0.05$, $n = 5$.

Gross phenotypes of *Nppc Fgfr3*^{ach} mice

To study the effects of CNP on dwarfism in *Fgfr3*^{ach} mice, we created *Fgfr3*^{ach} mice with targeted overexpression of CNP in cartilage by cross-mating *Fgfr3*^{ach} mice with *Nppc* mice. We confirmed the expression of the *Col2a1-Nppc* transgene in the cartilage of the resultant double transgenic (*Nppc Fgfr3*^{ach}) mice (data not shown). We also confirmed, by quantitative RT-PCR analysis, that the amount of *Fgfr3*^{ach} expression in the cartilage of *Nppc Fgfr3*^{ach} mice is no different from that in the cartilage of *Fgfr3*^{ach} mice, indicating that overexpression of CNP does not alter the expression of the *Fgfr3*^{ach} transgene (Fig. 2a).

The growth curve and soft x-ray analysis of *Nppc Fgfr3*^{ach} mice showed that the shortening of *Fgfr3*^{ach} mice is rescued by overexpression of CNP in the growth-plate cartilage (Fig. 2b,c). At the age of 10 weeks, the naso-anal length of *Nppc Fgfr3*^{ach} mice was 94.7 ± 4.0 mm, 8% larger than that of *Fgfr3*^{ach} mice (87.7 ± 2.6 mm) and comparable to that of their nontransgenic littermates (97.0 ± 4.2 mm) (Fig. 2b). The shortening of bones formed through endochondral ossification in 3-month-old female *Fgfr3*^{ach} mice, measured on the soft x-ray film, was rescued in *Nppc Fgfr3*^{ach} mice (Fig. 2d). The width of the cranium did not differ among the three genotypes (Fig. 2d).

To investigate the dose-response effect of CNP on the growth of achondroplastic bones, we generated *Fgfr3*^{ach} mice homozygous for the *Col2a1-Nppc* transgene. The relative abundance of CNP protein in the cartilage of neonatal mice, as estimated by immunohistochemical staining, was *Nppc*-homozygous *Fgfr3*^{ach} > *Nppc*-heterozygous *Fgfr3*^{ach} > *Fgfr3*^{ach} (Fig. 2e). The immunostaining intensities measured using NIH Image software[23] were 145% and 127% as high in the cartilage of *Nppc*-homozygous *Fgfr3*^{ach} and *Nppc*-heterozygous *Fgfr3*^{ach} mice, respectively, as in that of *Fgfr3*^{ach} mice. The dwarfing bones of *Fgfr3*^{ach} mice were elongated dose-dependently in *Nppc*-homozygous *Fgfr3*^{ach} and *Nppc*-heterozygous *Fgfr3*^{ach} mice (Fig. 2f).

Histological analysis of *Nppc Fgfr3*^{ach} mice

Microscopic analysis of tibial growth plates from 2-week-old mice showed that the decreased width of the growth plate of *Fgfr3*^{ach} mice (169 ± 15 μm) is rescued in *Nppc Fgfr3*^{ach} mice (229 ± 21 μm) and is comparable to that of their nontransgenic littermates (220 ± 15 μm) (Fig. 3a). Higher magnification showed that the decreased extracellular space between the proliferative and the upper hypertrophic chondrocyte layers of *Fgfr3*^{ach} mice was restored in *Nppc Fgfr3*^{ach} mice and could be as large as in nontransgenic littermates (Fig. 3b). *In situ* hybridization analysis showed that the width of the hypertrophic chondrocyte layer expressing *Col10a1* mRNA was also restored in *Nppc Fgfr3*^{ach} mice, although there was no appreciable difference in expression intensity between genotypes (see Supplementary Fig. 3 online). There was also no difference in the intensity of *Col2a1* mRNA expression (data not shown). In the proximal tibia of 2-week-old mice, the secondary ossification center was well organized in nontransgenic mice, whereas it was not yet formed in either their *Fgfr3*^{ach} or *Nppc Fgfr3*^{ach} littermates, indicating that overexpression of CNP does not affect the delayed differentiation of chondrocytes in achondroplastic growth plates (Fig. 3a). The secondary ossification centers in the tibiae of both *Fgfr3*^{ach} and *Nppc Fgfr3*^{ach} mice were formed about 3 d later than in nontransgenic tibia. The number of bromodeoxyuridine (BrdU)-positive chondrocytes was significantly lower in the growth plates of *Fgfr3*^{ach} mice, as previously reported[19], whereas there was no difference in the number of BrdU-positive chondrocytes in the growth plates of *Fgfr3*^{ach} and *Nppc Fgfr3*^{ach} mice (Fig. 3c and Supplementary Fig. 4 online). This indicates that overexpression of CNP does not change the decreased proliferation of chondrocytes in *Fgfr3*^{ach} mice.

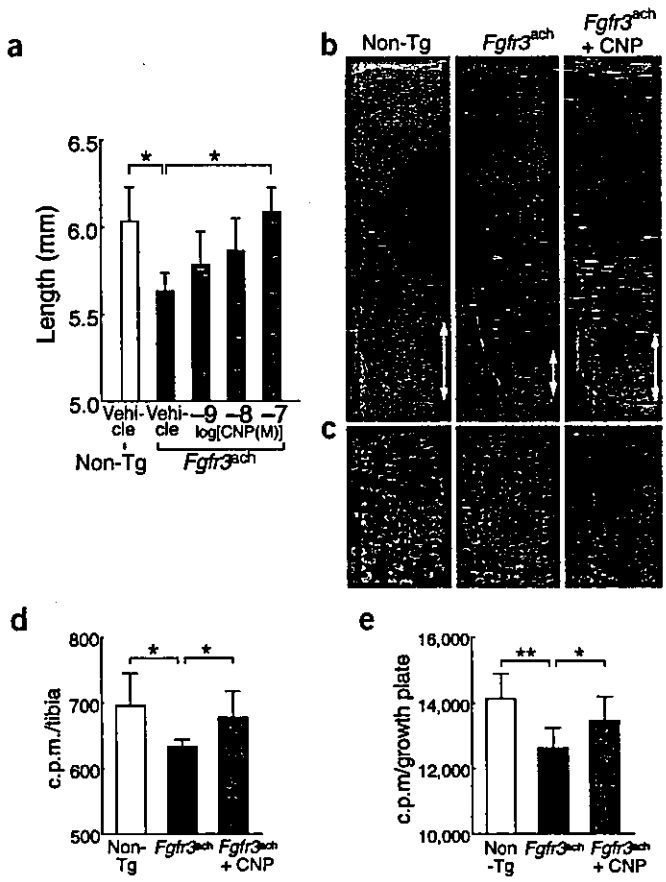

Figure 4 Effects of CNP on cultured tibiae from *Fgfr3*^{ach} mice. (**a**) Tibial lengths at the end of culture period. *, $P < 0.05$, $n = 5–6$. (**b**) Histological pictures of tibiae of nontransgenic mice, tibiae of *Fgfr3*^{ach} mice and CNP-treated tibiae of *Fgfr3*^{ach} mice. Arrows indicate the width of hypertrophic chondrocyte layers demarcated in the figures. (**c**) Highlight of the prehypertrophic chondrocyte layers from **b**. Scale bar, 200 μm (**b**) or 50 μm (**c**).(**d**,**e**) [^{35}S]sulfate (**d**) and [^{3}H]proline (**e**) incorporation into cartilage into tibiae of nontransgenic mice, *Fgfr3*^{ach} mice and *Fgfr3*^{ach} mice with CNP treatment. * and **, $P < 0.05$ and $P < 0.01$, respectively, $n = 5–6$ (**d**) and 9 (**e**).

Effects of CNP on cultured tibiae from *Fgfr3*^{ach} mice

To confirm the direct effect of CNP on bone growth in *Fgfr3*^{ach} mice, we carried out organ culture experiments using tibiae from fetal *Fgfr3*^{ach} mice. The fetal tibiae of *Fgfr3*^{ach} mice at 16.5 days post coitus (dpc) were shorter than those of their nontransgenic littermates (data not shown). CNP (10^{-9}–10^{-7} M) caused elongation of explanted tibiae from fetal *Fgfr3*^{ach} mice in a dose-dependent manner; those treated with 10^{-7} M CNP reached lengths as great as those of vehicle-treated tibiae from nontransgenic mice by the end of the culture period (Fig. 4a). Microscopic analysis showed that the width of the hypertrophic chondrocyte layer in cultured tibiae from *Fgfr3*^{ach} mice, which is lower than that in tibiae of nontransgenic mice, was restored by treatment with 10^{-7} M CNP (Fig. 4b). With higher magnification, we observed that the decreased extracellular space between the proliferative and the prehypertrophic chondrocyte layers of the tibiae of *Fgfr3*^{ach} mice was normalized by 10^{-7} M CNP (Fig. 4c). In fact, although the basal synthesis of glycosaminoglycan, measured by [^{35}S]sulfate incorporation, was much lower in tibiae from *Fgfr3*^{ach} mice than in those from nontransgenic mice, 10^{-7} M CNP increased glycosaminoglycan synthesis in tibiae from *Fgfr3*^{ach} mice to a level as high as in vehicle-treated tibiae from nontransgenic mice (Fig. 4d). The same dose of CNP also increased the synthesis of cartilage collagen, as estimated from the uptake of [^{3}H]proline into growth plates from *Fgfr3*^{ach} mice, to a level comparable to that in the growth plates from nontransgenic mice (Fig. 4e).

Effects of CNP on signaling pathways of FGF

We next investigated the effects of CNP on FGF signaling pathways in growth-plate chondrocytes using cultured tibiae from fetal mice. The treatment of tibial explants with CNP (10^{-6} and 10^{-7} M) or its second messenger, cGMP (10^{-5} M), before addition of FGF-2 (2 ng/ml) markedly decreased the FGF-2-induced phosphorylation of ERK1/2 in a dose-dependent fashion without decreasing the amount of ERK protein (Fig. 5a). In contrast, the same doses of either CNP or cGMP did not alter the FGF-2-induced phosphorylation of STAT-1 (Fig. 5b). Essentially identical results were obtained using the chondrogenic cell line ATDC5 (ref. 24) (data not shown). To further elucidate the effect of CNP on phosphorylation of ERK1/2 *in vivo*, we examined the amounts of phosphorylated ERK1/2 in the cartilage of nontransgenic, *Fgfr3*^{ach}, *Nppc* and *Nppc Fgfr3*^{ach} mice. The abundance of phosphorylated ERK1/2 was greater in the cartilage of *Fgfr3*^{ach} mice, and smaller in the cartilage of *Nppc* mice, than in the cartilage of nontransgenic mice. *Nppc Fgfr3*^{ach} mice, in which the shortening of achondroplastic bones was rescued, showed substantially less elevation of ERK1/2 phosphorylation than was seen in the cartilage of *Fgfr3*^{ach} mice (Fig. 5c). PD98059, an inhibitor of the MAPK cascade[25], increased the total length and width of the growth-plate cartilage of tibiae from both fetal *Fgfr3*^{ach} and nontransgenic mice in organ culture (Fig. 5d). PD98059 increased the length of tibiae from *Fgfr3*^{ach} mice more than that of tibiae from nontransgenic mice, in parallel with the level of cartilage matrix synthesis estimated from [^{35}S]sulfate and [^{3}H]proline incorporation (Fig. 5e–g). There was no difference in the proliferation of chondrocytes in tibiae, measured by BrdU uptake, between PD98059- and vehicle-treated groups of either genotype (labeling indexes: nontransgenic, 0.252 ± 0.029 versus 0.248 ± 0.025, respectively; *Fgfr3*^{ach}, 0.221 ± 0.025 versus 0.225 ± 0.027, respectively). We obtained the same results using U0126, another MEK inhibitor (data not shown).

DISCUSSION

This study demonstrates that targeted overexpression of CNP in cartilage counteracts dwarfism in *Fgfr3*^{ach} mice, a model of human achondroplasia. We previously showed, using transgenic and knockout mice, that the CNP–GC-B system is important in endochondral ossification[11–13]. The *Nppc* mice developed in this study showed skeletal overgrowth with widened growth plates, a phenotype resembling that of FGFR-3-depleted mice[17,18] and opposite to those of *Fgfr3*^{ach} mice[19] and *Nppc* knockout mice[13]. This indicates that the CNP–GC-B system may counteract the FGFs–FGFR-3 system in endochondral ossification. Here, we show that activation of the CNP–GC-B system reverses the FGFR-3-mediated inhibition of the endochondral ossification in achondroplasia. Activation of the CNP–GC-B system in chondrocytes of the growth plate therefore represents a potential new therapeutic strategy for human achondroplasia caused by a constitutively active mutation in *FGFR3*.

Constitutive activation of FGFR-3 has been reported to inhibit the growth of long bones made through endochondral ossification by decreasing the proliferation and delaying the differentiation of

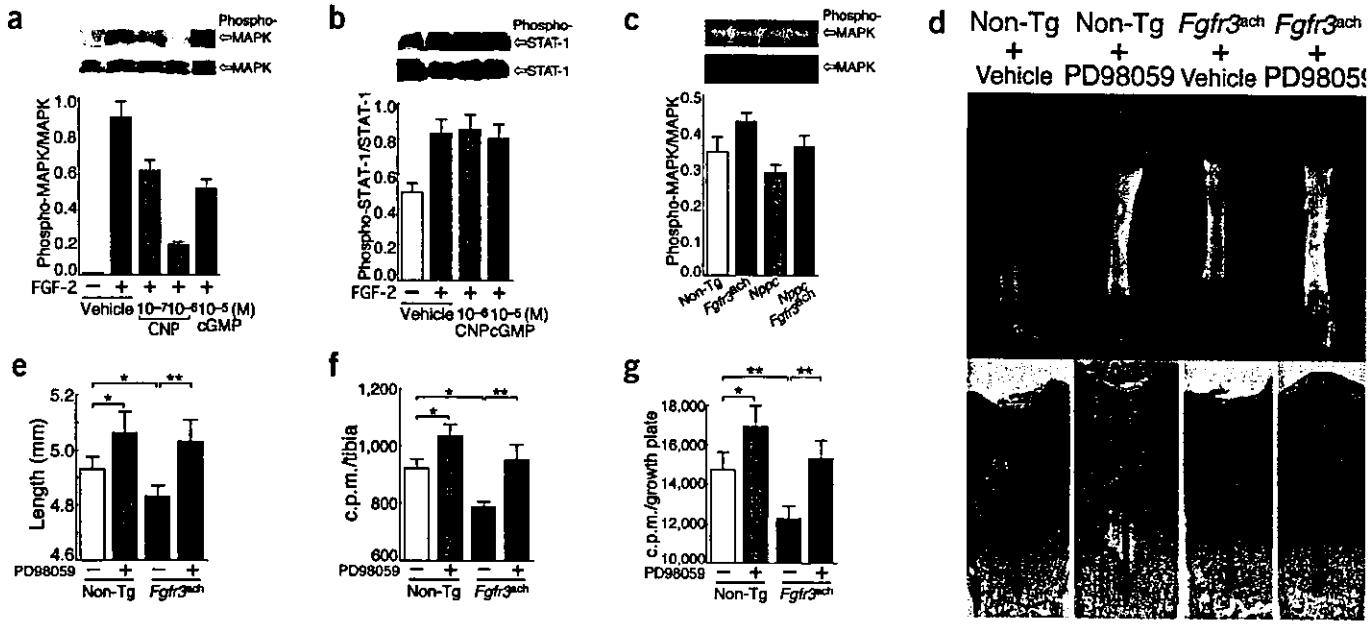

Figure 5 Intracellular signaling analysis. (**a–c**) Western blotting for phosphorylated MAPK (**a**) and STAT-1 (**b**) in explanted tibiae, and phosphorylated MAPK in growth-plate cartilage from neonatal mice (**c**). (**d–g**) Effects of PD98059 on cultured *Fgfr3*^{ach} tibiae. Gross appearance (upper) and histological picture of the growth plate (**d**), tibial length (**e**), [^{35}S]sulfate incorporation (**f**) and [^{3}H]proline uptake (**g**) in each group. Arrows in **d** indicate the width of the growth-plate cartilage. * and ** in **e–g**, $P < 0.05$ and $P < 0.01$, respectively, $n = 4–5$. Scale bar, 200 μm (**d**).

growth-plate chondrocytes via the STAT-1 pathway[6,19]. In the present study, however, we determined that CNP does not affect the amount of phosphorylated STAT-1 induced by FGF-2 either in explanted tibiae or in the chondrogenic cell line ATDC5. In addition, we showed that overexpressed CNP does not restore either the decreased BrdU uptake or the delayed formation of secondary ossification centers in the growth-plate cartilage of *Fgfr3*^{ach} mice (Fig. 3). Thus, CNP does not correct either the decreased proliferation or the delayed differentiation of achondroplastic growth-plate chondrocytes *in vivo*. These results show that CNP does not correct the STAT-1-mediated bone growth inhibition of activated FGFR-3. On the other hand, we show that constitutive activation of FGFR-3 inhibits longitudinal bone growth by decreasing the extracellular matrix synthesis through the MAPK pathway, indicating that MEK inhibitors (i) increase the extracellular matrix synthesis of explanted tibiae, as estimated by incorporation of [^{35}S]sulfate and [^{3}H]proline, more strongly in tibiae of *Fgfr3*^{ach} mice than in those of nontransgenic mice; (ii) do not alter the proliferation of chondrocytes, as estimated by BrdU uptake, in the tibiae of both *Fgfr3*^{ach} and nontransgenic mice; and (iii) elongate cultured tibiae from *Fgfr3*^{ach} mice more strongly than those from nontransgenic mice (Fig. 5e–g). In addition, we show that CNP markedly decreases the FGF-2-induced phosphorylation of ERK1/2 both in explanted tibiae and in ATDC5 cells, confirming that CNP interferes with activation of the MAPK pathway downstream of FGFR-3 signaling in the growth-plate cartilage, as we and other groups have previously reported in mesangeal cells[21] and fibroblasts[20]. We have further confirmed this finding using *in vivo* animal models, including *Nppc Fgfr3*^{ach} mice. Accordingly, we conclude that the mechanism by which CNP counteracts the dwarfism of achondroplastic bones in *Fgfr3*^{ach} mice is by restoring the MAPK-mediated inhibition of extracellular matrix production in the growth-plate cartilage of achondroplastic bones (Fig. 6). The role of the MAPK pathway in FGF signaling in chondrocytes has not been extensively studied so far, and the results of previous studies using cell culture were complicated and contradictory[26,27]. In the present study, we used both *ex vivo* organ culture and cell culture to elucidate the role of the MAPK pathway in endochondral bone elongation directly and in detail, and the two sets of results corresponded well. De Crombrugghe *et al.* have recently reported that constitutive activation of MEK1 in chondrocytes induces dwarfism that resembles achondroplasia (S. Murakami, S. McKinney, D. Givol, and B. de Crombrugghe, personal communication). These results support our hypothesis that the CNP–GC-B system rescues achondroplastic dwarfism by inhibiting the MAPK pathway of FGFR-3 signaling in the regulation of bone growth.

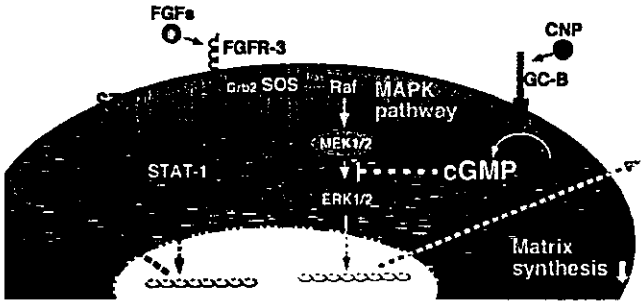

Figure 6 Schematic representation of the mechanism by which CNP compensates for FGFR-3-mediated shortening of bones. FGFR-3 inhibits endochondral bone growth by inhibiting proliferation and differentiation of growth-plate chondrocytes through the STAT-1 pathway and by decreasing extracellular matrix synthesis through the MAPK pathway. cGMP, the second messenger of CNP–GC-B, inhibits the MAPK pathway of FGFR-3 signaling, restores the decreased synthesis of the extracellular matrix and partially counteracts the dwarfism of achondroplastic bones.

Bone morphogenetic protein-2 (BMP-2) and BMP-4 have recently been reported to counteract the growth-inhibitory effect of FGFR-3 on explanted bones from the same achondroplastic model mice by restoring the proliferation of achondroplastic growth-plate chondrocytes[28]. Although the nature of intracellular interactions between FGF and BMP signaling in chondrocytes remains unclear, CNP and BMP might complementarily reverse the inhibitory effect of FGF on bone growth suggesting the possibility of a new combined therapy for achondroplasia.

Current therapies for achondroplasia include distraction osteogenesis[29,30], an orthopedic procedure, and administration of growth hormone[31]. Although distraction osteogenesis gives better results, it limits the quality of a patient's life. Growth hormone has only minimal effect on achondroplasia, has been reported to aggravate body disproportion in some case[32] and is very costly. According to our unpublished results, the maximal growth-promoting effect of CNP (10^{-7} M) on cultured fetal bones is much stronger than that of growth hormone (100 ng/ml), IGF-I (100 ng/ml)[33] or other skeletal growth regulators, including BMP-2 (100 ng/ml), BMP-4 (100 ng/ml), TGF-β_2 (100 ng/ml)[34] and PTH (100 ng/ml)[35], under identical experimental conditions. Activation of the CNP–GC-B system in chondrocytes may thus be a prospective means to treat achondroplasia. Activation of GC-B resulting from elevated plasma concentrations of BNP[11] or CNP (unpublished data) in transgenic mice using a promoter of serum amyloid P component causes skeletal overgrowth. This indicates that specific activators of the CNP–GC-B system could be delivered via the general circulation as therapy for achondroplasia. Considering the minimal hypotensive effect of CNP compared with the other natriuretic peptides ANP and BNP, systemic administration of CNP could be of practical use as a means to activate the CNP–GC-B system in the growth-plate chondrocytes. In addition, overexpression of CNP in cartilage increased bone mineral density, as estimated by pQCT, in the trabecular bone adjacent to the growth-plate cartilage, suggesting that the activation of the CNP–GC-B system in endochondral cartilage template formation positively affects the properties of bone produced from this template. This effect could be beneficial to patients with achondroplasia treated with CNP.

We observed a gender difference in the promoting effect of CNP on bone growth in the present study, but the reasons for this observation are unclear at present. Further studies are ongoing in our laboratory.

In conclusion, the present study demonstrates a potential new therapeutic strategy for human achondroplasia involving activation of the CNP–GC-B system in the chondrocytes of the growth plate.

METHODS

Generation and identification of *Nppc* mice. A 489-base-pair mouse *Nppc* cDNA[36] was inserted into a 6.5-kilobase segment of the *Col2a1* promoter region[22], at a site within the first intron. The assembled transgene (*Col2a1-Nppc*) was microinjected into fertilized C57BL/6 oocytes and the resultant transgenic mice were identified by Southern blotting. *Sac* I digestion of mouse genomic DNA containing *Col2a1-Nppc* yielded additional hybridizing DNA species of ~2.1 kilobases, whereas the intrinsic *Nppc* gene was recognized as DNA species of ~3.0 kilobases[37]. We assessed the transgene copy number on the basis of the density of the band compared with that of the intrinsic *Nppc* band as determined using densitometry.

Generation of the doubly transgenic mice of *Col2a1-Nppc* and *Fgfr3*^{ach}. Generation of transgenic mice that express an activated FGFR-3 in the growth plate (*Fgfr3*^{ach} mice) using *Col2a1* promoter and enhancer sequences was reported previously[19]. In all experiments using this achondroplastic model, we used transgenic mice carrying the heterozygous *Fgfr3*^{ach} transgene. To generate doubly transgenic mice for *Col2a1-Nppc* and *Fgfr3*^{ach}, *Nppc* mice were mated with *Fgfr3*^{ach} mice. The resultant *Nppc Fgfr3*^{ach} mice and *Nppc* mice were then mated to generate *Fgfr3*^{ach} mice homozygous for *Col2a1-Nppc*. All of the experimental procedures were approved by the Kyoto University Graduate School of Medicine committee on animal research.

Detection of mRNA expression of transgenes. To detect expression of *Col2a1-Nppc*, we carried out RT-PCR using as the forward primer a sequence located in the exon I of the *Col 2a1* gene and as the reverse primer a sequence from *Nppc* cDNA. The resultant PCR product of 450 base pairs was then recognizable as a transcript of the transgene from which the ~3-kilobase intron I of *Col2a1* had been spliced out. Expression of the *Fgfr3*^{ach} transgene was estimated by a quantitative RT-PCR method based on kinetic analysis[38,39], using primers for *Fgfr3*^{ach} and *Gapd*, as previously reported[19,39].

Skeletal morphology and pQCT analysis. For visualization of the whole skeleton, cleared skeletons of newborn mice were stained with Alizarin red S and Alcian blue[11]. To observe skeletons in adulthood, 3-month-old female mice were subjected to soft x-ray analysis[11], and the lengths of bones were measured on the soft x-ray film. To evaluate the bone mineral density of trabecular bones in the proximal tibiae, tibiae were subjected to pQCT analysis, using an XCT Research SA instrument (Stratec Medizintechnik), as previously reported[40].

Histological analysis. For light microscopy, sections were cut from paraffin-embedded specimens and stained with Alcian blue and hematoxylin-eosin (H&E). For BrdU staining, 2-week-old mice were injected intraperitoneally with BrdU (100 μg per gram body weight) and were killed 1 h later[19]. The labeling index in the proliferative chondrocyte layer was analyzed using National Institutes of Health (NIH) freeware. To evaluate the mineralized stage, von Kossa staining was done on undecalcified sections[13]. Immunohistochemical staining for CNP was carried out on frozen sections of neonatal mouse ribs using the ImmunoStaining Detection Kit (Peninsula). Intensity of immunostaining was analyzed using NIH freeware as previously described[23]. *In situ* hybridization analysis was carried out on 2-week-old mice tibiae using digoxigenin-labeled antisense and sense riboprobes obtained from rat *Col2a1* and *Col10a1* cDNA fragments[41].

Organ culture. Tibiae from *Fgfr3*^{ach} fetuses or their nontransgenic littermates were dissected out at 16.5 dpc and cultured for 4 d by the suspension culture technique[12] with the indicated doses of CNP or with biochemical inhibitors of MEK, PD98059 (50 μM, Cell Signaling) or U0126 (10 μM, Promega). Glycosaminoglycan synthesis in the cultured tibiae was assessed by measuring [^{35}S]sulfate incorporation as previously described[42], using 5 μCi/ml [^{35}S]sulfate in the medium. The synthesis of cartilage collagen was assessed by measuring uptake of [^{3}H]proline (20 μCi/ml in the medium) into cartilage collagen isolated from papain digests of the proximal tibial growth-plate cartilage[43]. The proliferation of chondrocytes in explanted tibiae was assessed by measuring BrdU incorporation as described before[12]. cGMP production was measured by radioimmunoassay[44] using cultured tibiae from *Nppc* or nontransgenic fetuses of 16.5 dpc at the end of the 4-d culture period.

Intracellular signaling analysis. Tibial explants from fetal mice of 16.5 dpc were incubated with 10^{-7}–10^{-6} M CNP or 10^{-5} M cGMP for 1 h, and then FGF-2 (2 ng/ml) was added for 5 min. ATDC5 cells on day 11 after confluency were incubated with the same doses of CNP or cGMP for 1 h, and then FGF-2 (1 ng/ml) was added for 3 min. Explanted tibiae, ATDC5 cells and tibial growth plates freshly dissected out from neonatal nontransgenic, *Fgfr3*^{ach}, *Nppc* and *Nppc Fgfr3*^{ach} mice were homogenized and lysed, and then western blotting was carried out using antibodies to phosphorylated ERK1/2 (Promega), ERK1/2 (BD Bioscience), phosphorylated STAT-1 (Cell Signaling) or STAT-1 (Santa Cruz Biotechnology).

Statistics. Data were expressed as mean ± s.d. and the statistical significance of differences in mean values was assessed by Student's *t*-test or analysis of variance (ANOVA) with Fisher's protected least-significant-difference test, as appropriate. Differences among means were considered significant at values of $P < 0.01$ or $P < 0.05$.

Note: Supplementary information is available on the Nature Medicine website.

ACKNOWLEDGMENTS

We thank D.M. Ornitz (Department of Molecular Biology and Pharmacology, Washington University School of Medicine) for *Fgfr3*^{ach} mice and B. DeCrombrugghe (Department of Molecular Genetics, University of Texas M.D. Anderson Cancer Center) for the *Col2a1* promoter. This work was supported by grants from Research for the Future of the Japan Society for the Promotion of Science (JSPS-RFTF 96100204 and 98L00801); the Japanese Ministry of Education, Sciences, Sports, and Culture (# 12770627); Smoking Research Foundation; Toyobo Biochemical Foundation; and Uehara Memorial Foundation.

COMPETING INTERESTS STATEMENT

The authors declare that they have no competing financial interests.

Received 29 September; accepted 26 November 2003
Published online at http://www.nature.com/naturemedicine/

1. Oberklaid, F., Danks, D.M., Jensen, F., Stace, L. & Rosshandler, S. Achondroplasia and hypochondroplasia. Comments on frequency, mutation rate, and radiological features in skull and spine. *J. Med. Genet.* **16**, 140–146 (1979).
2. Bellus, G.A. *et al.* Achondroplasia is defined by recurrent G380R mutations of FGFR3. *Am. J. Hum. Genet.* **56**, 368–373 (1995).
3. Shiang, R. *et al.* Mutations in the transmembrane domain of FGFR3 cause the most common genetic form of dwarfism, achondroplasia. *Cell* **78**, 335–342 (1994).
4. Cohen, M.M. Jr. Short-limb skeletal dysplasias and craniosynostosis: what do they have in common? *Pediatr. Radiol.* **27**, 442–446 (1997).
5. Boilly, B., Vercoutter-Edouart, A.S., Hondermarck, H., Nurcombe, V. & Le Bourhis, X. FGF signals for cell proliferation and migration through different pathways. *Cytokine Growth Factor Rev.* **11**, 295–302 (2000).
6. Sahni, M. *et al.* FGF signaling inhibits chondrocyte proliferation and regulates bone development through the STAT-1 pathway. *Genes Dev.* **13**, 1361–1366 (1999).
7. Sahni, M., Raz, R., Coffin, J.D., Levy, D. & Basilico, C. STAT1 mediates the increased apoptosis and reduced chondrocyte proliferation in mice overexpressing FGF2. *Development* **128**, 2119–2129 (2001).
8. Nakao, K., Ogawa, Y., Suga, S. & Imura, H. Molecular biology and biochemistry of the natriuretic peptide system. I: Natriuretic peptides. *J. Hypertens.* **10**, 907–912 (1992).
9. Nakao, K., Ogawa, Y., Suga, S. & Imura, H. Molecular biology and biochemistry of the natriuretic peptide system. II: Natriuretic peptide receptors. *J. Hypertens.* **10**, 1111–1114 (1992).
10. Garbers, D.L. Guanylate cyclase receptor family. *Recent. Prog. Horm. Res.* **46**, 85–96 (1990).
11. Suda, M. *et al.* Skeletal overgrowth in transgenic mice that overexpress brain natriuretic peptide. *Proc. Natl. Acad. Sci. USA* **95**, 2337–2342 (1998).
12. Yasoda, A. *et al.* Natriuretic peptide regulation of endochondral ossification. Evidence for possible roles of the C-type natriuretic peptide/guanylyl cyclase-B pathway. *J. Biol. Chem.* **273**, 11695–11700 (1998).
13. Chusho, H. *et al.* Dwarfism and early death in mice lacking C-type natriuretic peptide. *Proc. Natl. Acad. Sci. USA* **98**, 4016–4021 (2001).
14. Pfeifer, A. *et al.* Intestinal secretory defects and dwarfism in mice lacking cGMP-dependent protein kinase II. *Science* **274**, 2082–2086 (1996).
15. Matsukawa, N. *et al.* The natriuretic peptide clearance receptor locally modulates the physiological effects of the natriuretic peptide system. *Proc. Natl. Acad. Sci. USA* **96**, 7403–7408 (1999).
16. Jaubert, J. *et al.* Three new allelic mouse mutations that cause skeletal overgrowth involve the natriuretic peptide receptor C gene (Npr3). *Proc. Natl. Acad. Sci. USA* **96**, 10278–10283 (1999).
17. Colvin, J.S., Bohne, B.A., Harding, G.W., McEwen, D.G. & Ornitz, D.M. Skeletal overgrowth and deafness in mice lacking fibroblast growth factor receptor 3. *Nat. Genet.* **12**, 390–397 (1996).
18. Deng, C., Wynshaw-Boris, A., Zhou, F., Kuo, A. & Leder, P. Fibroblast growth factor receptor 3 is a negative regulator of bone growth. *Cell* **84**, 911–921 (1996).
19. Naski, M.C., Colvin, J.S., Coffin, J.D. & Ornitz, D.M. Repression of hedgehog signaling and BMP4 expression in growth plate cartilage by fibroblast growth factor receptor 3. *Development* **125**, 4977–4988 (1998).
20. Chrisman, T.D. & Garbers, D.L. Reciprocal antagonism coordinates C-type natriuretic peptide and mitogen-signaling pathways in fibroblasts. *J. Biol. Chem.* **274**, 4293–4299 (1999).
21. Suganami, T. *et al.* Overexpression of brain natriuretic peptide in mice ameliorates immune-mediated renal injury. *J. Am. Soc. Nephrol.* **12**, 2652–2663 (2001).
22. Metsaranta, M. *et al.* Developmental expression of a type II collagen/β-galactosidase fusion gene in transgenic mice. *Dev. Dyn.* **204**, 202–210 (1995).
23. Toyokuni, S. *et al.* Quantitative immunohistochemical determination of 8-hydroxy-2'-deoxyguanosine by a monoclonal antibody N45.1: its application to ferric nitrilotriacetate-induced renal carcinogenesis model. *Lab. Invest.* **76**, 365–374 (1997).
24. Shukunami, C. *et al.* Chondrogenic differentiation of clonal mouse embryonic cell line ATDC5 *in vitro*: differentiation-dependent gene expression of parathyroid hormone (PTH)/PTH-related peptide receptor. *J. Cell. Biol.* **133**, 457–468 (1996).
25. Dudley, D.T., Pang, L., Decker, S.J., Bridges, A.J. & Saltiel, A.R. A synthetic inhibitor of the mitogen-activated protein kinase cascade. *Proc. Natl. Acad. Sci. USA* **92**, 7686–7689 (1995).
26. Murakami, S., Kan, M., McKeehan, W.L. & de Crombrugghe, B. Up-regulation of the chondrogenic Sox9 gene by fibroblast growth factors is mediated by the mitogen-activated protein kinase pathway. *Proc. Natl. Acad. Sci. USA* **97**, 1113–1118 (2000).
27. Yoon, Y.M. *et al.* Maintenance of differentiated phenotype of articular chondrocytes by protein kinase C and extracellular signal-regulated protein kinase. *J. Biol. Chem.* **277**, 8412–8420 (2002).
28. Minina, E., Kreschel, C., Naski, M.C., Ornitz, D.M. & Vortkamp, A. Interaction of FGF, Ihh/Pthlh, and BMP signaling integrates chondrocyte proliferation and hypertrophic differentiation. *Dev. Cell* **3**, 439–449 (2002).
29. Noonan, K.J., Leyes, M., Forriol, F. & Canadell, J. Distraction osteogenesis of the lower extremity with use of monolateral external fixation. A study of two hundred and sixty-one femora and tibiae. *J. Bone. Joint. Surg. Am.* **80**, 793–806 (1998).
30. Aldegheri, R. Distraction osteogenesis for lengthening of the tibia in patients who have limb-length discrepancy or short stature. *J. Bone. Joint. Surg. Am.* **81**, 624–634 (1999).
31. Tanaka, H. *et al.* Effect of growth hormone therapy in children with achondroplasia: growth pattern, hypothalamic-pituitary function, and genotype. *Eur. J. Endocrinol.* **138**, 275–280 (1998).
32. Kanaka-Gantenbein, C. Present status of the use of growth hormone in short children with bone diseases (diseases of the skeleton). *J. Pediatr. Endocrinol. Metab.* **14**, 17–26 (2001).
33. Scheven, B.A. & Hamilton, N.J. Longitudinal bone growth *in vitro*: effects of insulin-like growth factor I and growth hormone. *Acta Endocrinol.* **124**, 602–607 (1991).
34. Dieudonne, S.C. *et al.* Opposite effects of osteogenic protein and transforming growth factor β on chondrogenesis in cultured long bone rudiments. *J. Bone Miner. Res.* **9**, 771–780 (1994).
35. Coxam, V., Miller, M.A., Bowman, B.M., Qi, D. & Miller, S.C. Insulin-like growth factor 1 and parathyroid hormone effects on the growth of fetal rat metatarsal bones cultured in serum-free medium. *Biol. Neonate.* **68**, 368–376 (1995).
36. Kojima, M., Minamino, N., Kangawa, K. & Matsuo, H. Cloning and sequence analysis of a cDNA encoding a precursor for rat C-type natriuretic peptide (CNP). *FEBS Lett.* **276**, 209–213 (1990).
37. Ogawa, Y. *et al.* Molecular cloning and chromosomal assignment of the mouse C-type natriuretic peptide (CNP) gene (Nppc): comparison with the human CNP gene (NPPC). *Genomics* **24**, 383–387 (1994).
38. Nakayama, H., Yokoi, H. & Fujita, J. Quantification of mRNA by non-radioactive RT-PCR and CCD imaging system. *Nucleic Acids Res.* **20**, 4939 (1992).
39. Yokoi, H. *et al.* Non-radioisotopic quantitative RT-PCR to detect changes in mRNA levels during early mouse embryo development. *Biochem. Biophys. Res. Commun.* **195**, 769–775 (1993).
40. Liu, W. *et al.* Overexpression of Cbfa1 in osteoblasts inhibits osteoblast maturation and causes osteopenia with multiple fractures. *J. Cell. Biol.* **155**, 157–166 (2001).
41. Chusho, H. *et al.* Genetic models reveal that brain natriuretic peptide can signal through different tissue-specific receptor-mediated pathways. *Endocrinology* **141**, 3807–3813 (2000).
42. Mericq, V., Uyeda, J.A., Barnes, K.M., De Luca, F. & Baron, J. Regulation of fetal rat bone growth by C-type natriuretic peptide and cGMP. *Pediatr. Res.* **47**, 189–193 (2000).
43. Bonassar, L.J., Grodzinsky, A.J., Srinivasan, A., Davila, S.G. & Trippel, S.B. Mechanical and physicochemical regulation of the action of insulin-like growth factor-I on articular cartilage. *Arch. Biochem. Biophys.* **379**, 57–63 (2000).
44. Maack, T. *et al.* Physiological role of silent receptors of atrial natriuretic factor. *Science* **238**, 675–678 (1987).

Significance and therapeutic potential of the natriuretic peptides/cGMP/cGMP-dependent protein kinase pathway in vascular regeneration

Kenichi Yamahara*, Hiroshi Itoh*†, Tae-Hwa Chun*, Yoshihiro Ogawa*, Jun Yamashita*, Naoki Sawada*, Yasutomo Fukunaga*, Masakatsu Sone*, Takami Yurugi-Kobayashi*, Kazutoshi Miyashita*, Hirokazu Tsujimoto*, Hyun Kook‡, Robert Feil§, David L. Garbers¶, Franz Hofmann§, and Kazuwa Nakao*

*Department of Medicine and Clinical Science, Kyoto University Graduate School of Medicine, Kyoto 606-8507, Japan; ‡Research Institute of Medical Sciences, Chonnan National University Medical School, Gwangju 501-746, Republic of Korea; §Institut für Pharmakologie und Toxikologie, Technische Universität München, Munich 80802, Germany; ¶Cecil H. and Ida Green Center for Reproductive Biology Sciences, Howard Hughes Medical Institute, Department of Pharmacology, University of Texas Southwestern Medical Center, Dallas, TX 75390

Contributed by David L. Garbers, December 31, 2002

Natriuretic peptides (NPs), which consist of atrial, brain, and C-type natriuretic peptides (ANP, BNP, and CNP, respectively), are characterized as cardiac or vascular hormones that elicit their biological effects by activation of the cGMP/cGMP-dependent protein kinase (cGK) pathway. We recently reported that adenoviral gene transfer of CNP into rabbit blood vessels not only suppressed neointimal formation but also accelerated reendothelialization, a required step for endothelium-dependent vasorelaxation and antithrombogenicity. Accordingly, we investigated the therapeutic potential of the NPs/cGMP/cGK pathway for vascular regeneration. In transgenic (Tg) mice that overexpress BNP in response to hindlimb ischemia, neovascularization with appropriate mural cell coating was accelerated without edema or bleeding, and impaired angiogenesis by the suppression of nitric oxide production was effectively rescued. Furthermore, in BNP-Tg mice, inflammatory cell infiltration in ischemic tissue and vascular superoxide production were suppressed compared with control mice. Ischemia-induced angiogenesis was also significantly potentiated in cGK type I Tg mice, but attenuated in cGK type I knockout mice. NPs significantly stimulated capillary network formation of cultured endothelial cells by cGK stimulation and subsequent Erk1/2 activation. Furthermore, gene transfer of CNP into ischemic muscles effectively accelerated angiogenesis. These findings reveal an action of the NPs/cGMP/cGK pathway to exert multiple vasculoprotective and regenerative actions in the absence of apparent adverse effects, and therefore suggest that NPs as the endogenous cardiovascular hormone can be used as a strategy of therapeutic angiogenesis in patients with tissue ischemia.

Natriuretic peptides (NPs) consist of atrial NP (ANP), brain NP (BNP), and C-type NP (CNP). They share the same intracellular signal transduction pathway for cGMP/cGMP-dependent protein kinase (cGK) as nitric oxide (NO). We have demonstrated that ANP and BNP are cardiac hormones that are produced mainly in the atrium and ventricle, respectively (1, 2). CNP, in contrast, is produced in and secreted from endothelial cells (ECs) to act as a local regulator of vascular tone and growth (3).

We recently reported that in both rabbit balloon injury and vein graft models, overexpression of the CNP gene by adenoviral vector accelerated reendothelialization and inhibited vascular smooth muscle proliferation (4, 5). This finding indicates the complex responses to NPs in different types of vascular cells, both ECs and smooth muscle cells (SMCs).

A large body of literature indicates an essential role of endothelial NO for angiogenesis. Previous studies demonstrated that vascular endothelial growth factor (VEGF) stimulates Akt/protein kinase B (6, 7), which has been shown to phosphorylate endothelial NO synthase, leading to its activation (8, 9). VEGF-stimulated proliferation of cultured ECs, triggered by endothelial NO synthase activation (10), was also shown to require intracellular signaling through cGK, Raf-1 kinase, and Erk1/2 (11, 12). Based on these findings, we hypothesized that NPs could promote vascular regeneration. To examine this hypothesis, we used a mouse model of operatively induced hindlimb ischemia (13) to investigate the effects of NPs on angiogenesis by using transgenic (Tg) mice that overexpress BNP (14) with or without N^{ω}-nitro-L-arginine methyl ester (L-NAME), an inhibitor of NO synthase. We also applied this model to both cGK type I (cGKI)-knockout (15) and Tg mice to investigate the impact of cGKI, one of the cGK isoforms, which is present in ECs and SMCs. Finally, we examined the effect of CNP on angiogenesis by a gene-transfer approach to seek the therapeutic potentials of NPs in vascular regeneration. The present study elucidates the action of the NPs/cGMP/cGKI pathway on angiogenesis and provides a strategy for therapeutic angiogenesis by using an endogenous cardiovascular hormone to exert vasculoprotective and vasculoregenerative actions in the absence of apparent adverse effects.

Materials and Methods

BNP-Tg Mice. Generation of BNP-Tg mice (line 55) was reported (14). BNP-Tg showed a marked increase in plasma BNP levels ($1.8 \pm 1.1 \times 10^{-9}$ M) compared with their control littermates (non-Tg) ($<0.06 \times 10^{-9}$ M; refs. 14 and 16). These mice (10–15 wk) were randomly allotted to four treatment groups: BNP-Tg and non-Tg, with or without L-NAME (Nacalai Tesque, Kyoto) administration (200 mg/liter in drinking water; ref. 17).

cGKI-Knockout Mice. We developed mice with targeted disruption of the cGKI gene (15). We used homozygous cGKI mutant mice ($cGKI^{-/-}$), heterozygous mutant mice ($cGKI^{+/-}$), and their control littermates ($cGK^{+/+}$) (10–15 wk).

cGKI-Tg Mice. We generated cGKI-Tg mice (T.-H.C. and H.I., unpublished data). Briefly, the cDNA coding for human cGKIα, which we cloned (18), was subcloned into the expression vector pCXN2 (19), driven by the CAG promoter (pCXN2-hcGKIα). The fragment of pCXN2-hcGKIα was microinjected into a C57BL/6 mouse. We used mice with 15 copies of the transgene and their control littermates at the age of 10–15 wk. To confirm cGKI expression in cGKI-Tg mice, Northern blot analysis was

Abbreviations: NP, natriuretic peptide; ANP, atrial NP; BNP, brain NP; CNP, C-type NP; cGK, cGMP-dependent protein kinase; EC, endothelial cell; SMC, smooth muscle cell; Tg, transgenic; L-NAME, N^{ω}-nitro-L-arginine methyl ester; LDPI, laser Doppler perfusion image; PECAM-1, platelet EC adhesion molecule-1; SMA, smooth muscle actin, GC, guanylyl cyclase; VEGF, vascular endothelial growth factor.

†To whom correspondence should be addressed at: Department of Medicine and Clinical Science, Kyoto University Graduate School of Medicine, 54 Shogoin Kawahara-cho, Sakyo-ku, Kyoto 606-8507, Japan. E-mail: hiito@kuhp.kyoto-u.ac.jp.

www.pnas.org/cgi/doi/10.1073/pnas.0538059100

performed with a human cGKIα-specific probe, a 311-bp-long fragment at the 5′ end sequence released by pCXN2-hcGKIα.

Ligation Model. After being anesthetized with pentobarbital (80 mg/kg, i.p.), the right femoral artery and vein were exposed, dissected free, and excised (13). Experimental procedures were performed according to Kyoto University standards for animal care.

Hindlimb blood flow was assessed with a laser Doppler perfusion image (LDPI) analyzer (Moor Instruments, Devon, U.K.) as described (13).

Immunohistochemistry. After fixation with 4% paraformaldehyde, ischemic lower legs were embedded in OCT compound (Sakura Finetechnical, Tokyo) and frozen at −80°C. Cryostat sections (4–8 μm thick) of the tissues were stained with rat anti-mouse platelet EC adhesion molecule-1 (PECAM-1) (PharMingen), mouse anti-α smooth muscle actin (SMA) (Sigma), rat anti-mouse CD45 (PharMingen), rabbit anti-cGKI (Calbiochem), rabbit anti-guanylyl cyclase A (GC-A) and B (GC-B) antibody that we developed (20), rabbit anti-Erk1/2 and phospho-Erk1/2 (Thr-202/Tyr-204) antibody (Cell Signaling Technology, Beverly, MA), or mouse anti-CNP antibody that we developed (KY-CNP-1; ref. 21). As the negative control, rabbit preimmune serum or normal Ig fraction (DAKO) was used to show antibody specificity.

Analysis of Capillary Density and Inflammation. Four random fields on two different sections (≈3 mm apart) from each mouse were photographed with a digital camera (Olympus, Tokyo). By computer-assisted analysis using NIH IMAGE, capillary density was calculated as the mean number of capillaries stained with PECAM-1 (endothelial marker) or α SMA (vascular smooth muscle marker), and the mean number of infiltrating CD45-positive leukocytes was counted as the assessment of inflammation.

Evaluation of *in Situ* Reactive Oxygen Production. The oxidative fluorescent dye dihydroethidium (2×10^{-6} M) was used to evaluate the *in situ* concentration of superoxide in ischemic hindlimb tissue, as described (22). We also stained 4-hydroxy-2-nonenal (4-HNE) (Nippon Oil & Fats, Tokyo), an unsaturated aldehyde that can be formed by the peroxidation of unsaturated fatty acids, such as linoleic and arachidonic acids (23).

Capillary Network Formation Assay. Human umbilical vein ECs (Clonetics, Walkersville, MD) were grown in basic medium (EBM2) (Clonetics) containing growth supplements (EGM2) (Clonetics). They (two to three passages, 4×10^4 cells per well) were seeded at Matrigel-coated Cellware 24-well plates (Becton Dickinson) and incubated for 1 h in 100 μl of EBM2 containing 10% FBS. Serum-free medium (400 μl) containing human ANP, BNP, and CNP (Peptide Institute, Osaka) with or without Rp-8-pCPT-cGMP/PD98059 (Calbiochem) were added. After a 10-h incubation, they were fixed with 10% buffered formalin. Two random fields of view in three or four replicate wells were visualized, and images were captured by using the Olympus digital camera. Network formation was assessed by calculating the total area covered by capillaries in each field of view using NIH IMAGE.

Construction of CNP Plasmid and Its Administration to Ligation Model. The full length of rat CNP cDNA (384 bp) was inserted into the pAC-CMVpLpA vector (4). The plasmid DNA was prepared from cultures of pAC-CMVpLpA-transformed *Escherichia coli* by the EndoFree Plasmid Kit (Qiagen, Valencia, CA). After mouse femoral artery ligation, a local injection of plasmid carrying the CNP cDNA (pAC.CMV/CNP) or none (pAC.CMV) was performed (500 μg per mouse in 200 μl of PBS in 10 injection sites). Plasma CNP level was confirmed by an EIA (Phoenix Pharmaceuticals, St. Joseph, MO).

Statistical Analysis. Results are presented as means ± SEM. The statistical significance of differences in the studies was evaluated by ANOVA. A P value < 0.05 was considered significant.

Results

Ischemia-Induced Angiogenesis Was Accelerated in BNP-Tg Mice. Serial blood flow measurements by LDPI revealed that accelerated limb perfusion improvement was observed for up to 12 days in BNP-Tg mice compared with non-Tg mice (Fig. 1 *a* and *b*). The calculated perfusion ratio of ischemic to nonischemic hindlimb was 0.12 ± 0.02 for BNP-Tg vs. 0.06 ± 0.01 for non-Tg at day 4 ($P = 0.002$), 0.46 ± 0.06 vs. 0.24 ± 0.05 at day 8 ($P = 0.006$), and 0.61 ± 0.07 vs. 0.45 ± 0.04 at day 12 ($P = 0.04$), respectively. After 14 days, restoration of perfusion in BNP-Tg mice was close to non-Tg mice, and no significant difference was seen.

Compatible with the result of blood flow measurement, capillary density in the BNP-Tg group (2,265 ± 62 per mm^2) at 10 days was significantly higher than that of the non-Tg group (1,778 ± 74 per mm^2; $P < 0.0001$; Fig. 1 *e* and *f*). At day 28, capillary density was equivalent in both groups (Fig. 1 *g* and *h*).

Overexpression of BNP Restored Delayed Angiogenesis Induced by NO Blockade. L-NAME administration to non-Tg mice disclosed impaired recovery in hindlimb perfusion compared with the non-Tg without L-NAME group (Fig. 1*c*). The ratio of ischemic/normal blood flow measured at 14 days was 0.37 ± 0.04 for the non-Tg (+L-NAME) and significantly lower compared with 0.43 ± 0.03 for the non-Tg alone ($P = 0.015$). After 14 days, the ratio of both groups became similar.

In contrast to non-Tg, L-NAME administration had no significant effect on the ratio of blood perfusion in BNP-Tg at any time point (Fig. 1*d*).

On day 10, capillary density of L-NAME-treated non-Tg mice (1,516 ± 62 per mm^2) was lower than that of untreated non-Tg mice ($P = 0.014$; Fig. 1 *e* and *f*). In contrast, no difference was seen in BNP-Tg with (2,113 ± 27 per mm^2) or without L-NAME administration (day 10). Capillary density in the L-NAME-treated BNP-Tg group was significantly higher than that of the L-NAME-treated non-Tg group ($P = 0.023$) (day 10). On day 28, capillary density was equivalent in these four groups (Fig. 1 *g* and *h*).

Maturity of Newly Formed Blood Vessels in BNP-Tg Mice. From double immunostaining of ischemic hindlimb tissue with PECAM-1 and α SMA, the structure of capillaries (ECs with adhering mural cells) showed no apparent difference between BNP-Tg and non-Tg mice (data not shown). Accordingly, immunostaining of the ischemic hindlimb tissues at day 10 with anti-αSMA antibody revealed significantly increased α SMA-positive capillary density in BNP-Tg mice (2,061 ± 65 per mm^2) compared with non-Tg mice (1,578 ± 79 per mm^2; $P = 0.0001$; Fig. 2 *a* and *b*). In addition, edema or bleeding in the ischemic hindlimb tissues was not observed in BNP-Tg mice.

Focal Inflammation in BNP-Tg Mice. In both BNP-Tg and non-Tg mice, the number of CD45-positive infiltrating leukocytes of the ischemic hindlimb tissues increased until day 5, then gradually decreased (Fig. 2*c*). At day 7, infiltrating leukocytes in BNP-Tg mice were significantly lower than those of non-Tg mice ($P = 0.002$), and no significant difference was seen at days 3, 5, and 10.

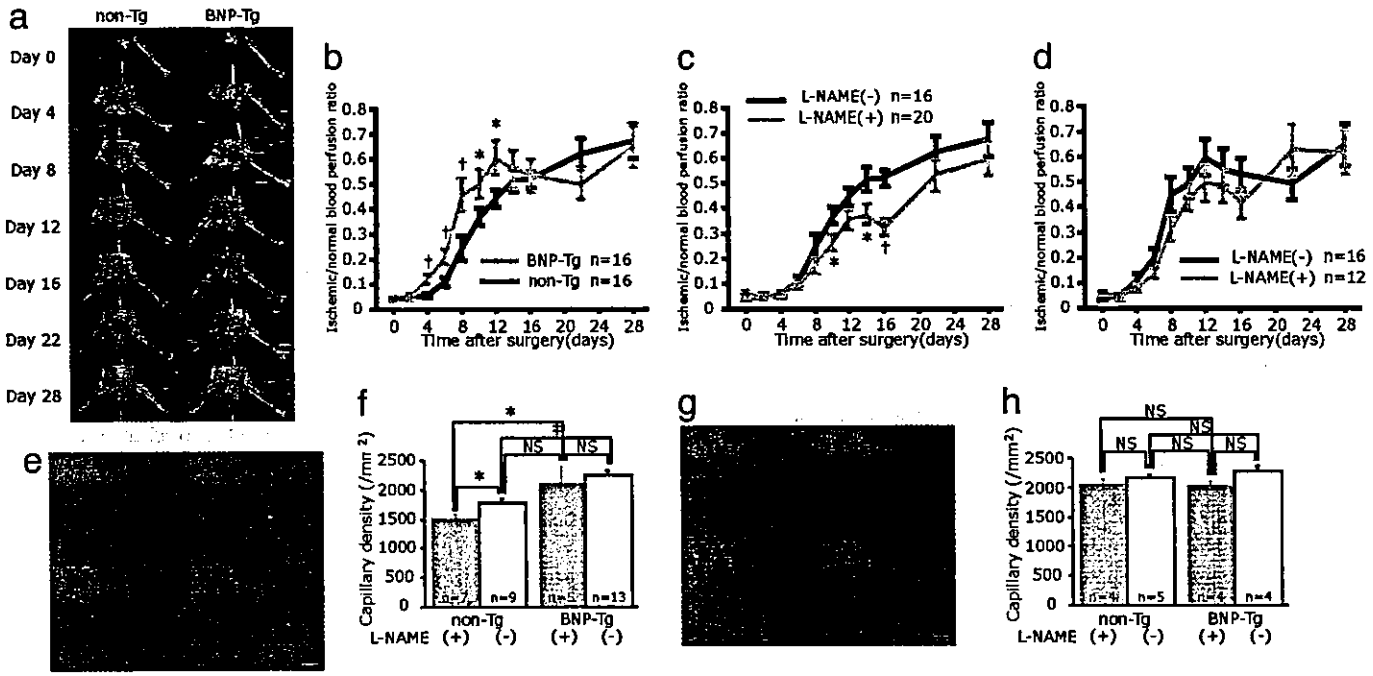

Fig. 1. Ischemia-induced angiogenesis was accelerated in BNP-Tg mice, and overexpression of BNP restored delayed angiogenesis induced by NO blockade. (*a*) Serial LDPI analysis of hindlimb ischemia in BNP-Tg and non-Tg mice. (*b*) Quantitative analysis of ischemic/normal hindlimb perfusion ratio in BNP-Tg and non-Tg mice. (*c* and *d*) Serial LDPI measurements in non-Tg (*c*) and BNP-Tg (*d*) mice with and without L-NAME treatment. (*e* and *g*) Immunostaining of the ischemic hindlimb tissues with anti-PECAM-1 antibody (bright red) at day 10 (*e*) and day 28 (*g*). (*f* and *h*) Quantitative analysis of capillary density at day 10 (*f*) and day 28 (*h*). *, $P < 0.05$; †, $P < 0.01$; ‡, $P < 0.001$; NS, not significant. (Scale bar, 100 μm.)

Reactive Oxygen Production in Blood Vessels of Ischemic Hindlimb Tissue. By dihydroethidium staining of ischemic hindlimb tissue at day 7, *in situ* concentration of superoxide in the blood vessels of BNP-Tg mice was obviously lower than that of non-Tg mice (Fig. 2*d*). Furthermore, immunostaining of 4-HNE demonstrated that reactive oxygen production was also suppressed in

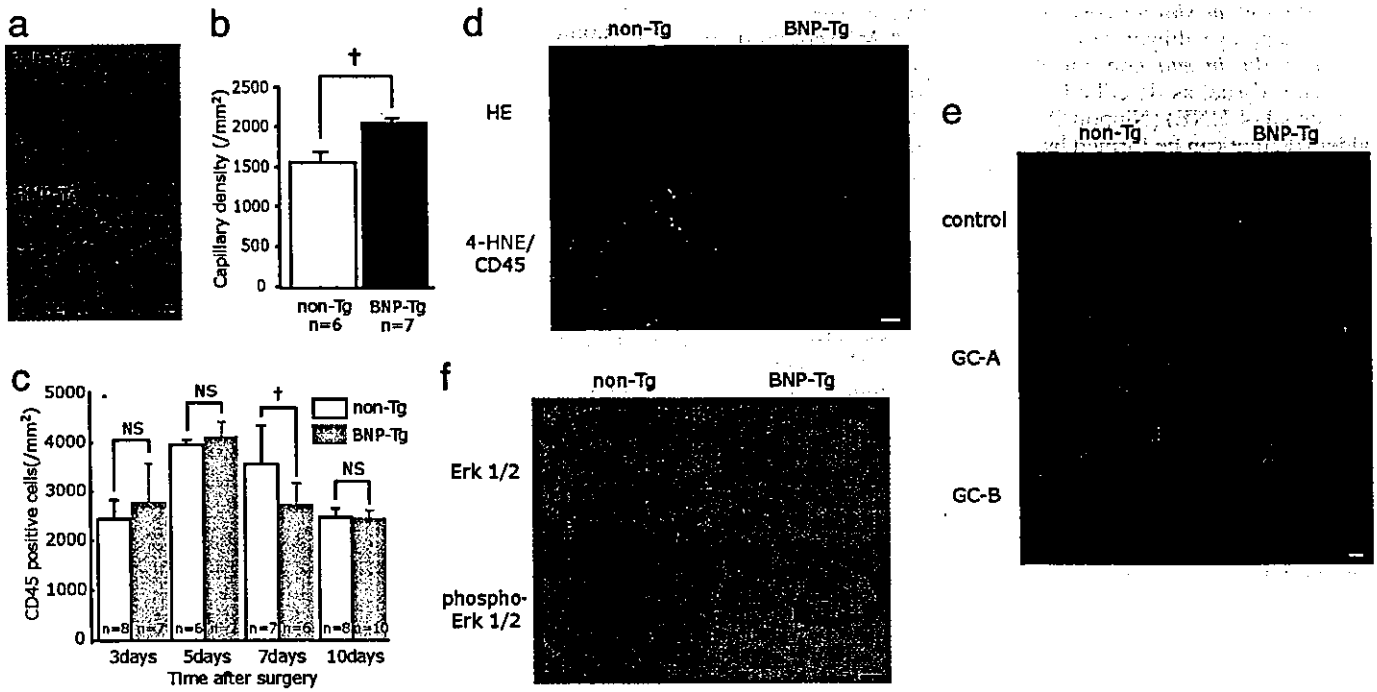

Fig. 2. Evaluation of ischemic hindlimb tissue of BNP-Tg mice. (*a* and *b*) α SMA staining (purple) of the ischemic hindlimb tissues at day 10 (*a*) and quantitative analysis of capillary density (*b*). (*c*) Time course of focal inflammation of ischemic hindlimb obtained from immunostaining with anti-CD45 antibody. (*d*) Dihydroethidium (HE) staining (*Upper*; red) and 4-hydroxy-2-nonenal (4-HNE)/CD45 staining (*Lower*; green fluorescence/red) of the ischemic hindlimb tissue at day 7. (*e*) Expression of GC-A and GC-B (green fluorescence) in the ischemic hindlimb at day 7. Negative controls for these antibodies are also shown. (*f*) Immunostaining of the ischemic hindlimb tissues at day 7 with anti-Erk1/2 or phosphor-Erk1/2 antibody (brown). †, $P < 0.01$. (Scale bars: *a*, 100 μm; *d–f*, 25 μm.)

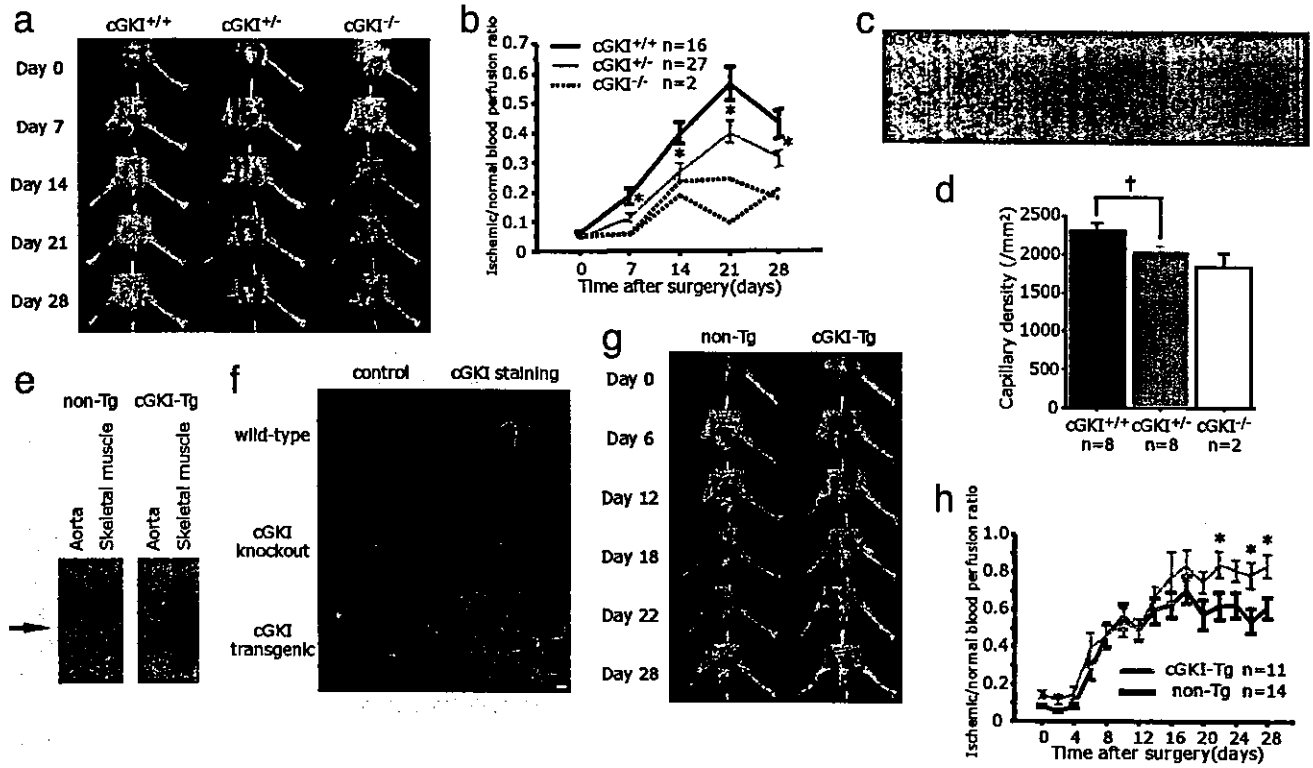

Fig. 3. Angiogenesis was blunted in cGKI-knockout mice and accelerated in cGKI-Tg mice. (*a* and *b*) Serial LDPI measurements in cGKI-knockout mice. (*c* and *d*) PECAM-1 staining (bright red) of the ischemic hindlimb tissues at day 28 in cGKI-Tg mice (*c*) and quantitative analysis of capillary density (*d*). (*e*) The expression of cGKI mRNA in non-Tg and cGKI-Tg mice. (*f*) Immunostaining of cGKI (green fluorescence) with their negative control in WT, cGKI-knockout, and cGKI-Tg mice. (*g* and *h*) Serial LDPI measurements in cGKI-Tg mice. *, $P < 0.05$; †, $P < 0.01$. (Scale bars: *c*, 100 μm; *f*, 25 μm.)

BNP-Tg. From double immunostaining with CD45 in non-Tg mice, reactive oxygen production was prominent in infiltrating leukocytes around and within the blood vessels, as well as SMCs. In BNP-Tg mice, the number of reactive oxygen-positive inflammatory cells was decreased and reactive oxygen production in SMCs was diminished.

Expression of GC-A and GC-B in Ischemic Hindlimb Tissue. Immunostaining (after antigen retrieval) of these receptors in ischemic hindlimb tissue at day 7 revealed that GC-A and GC-B were similarly expressed in the blood vessels of both BNP-Tg and non-Tg mice (Fig. 2*e*). Negative controls showed virtually no significant staining in these serial sections.

Expression of Erk1/2 and Phospho-Erk1/2 in Ischemic Hindlimb Tissue. By immunostaining of Erk1/2 in ischemic hindlimb tissue at day 7, Erk1/2 was equally expressed in ECs and SMCs of both BNP-Tg and non-Tg mice. On the other hand, the expression of phospho-Erk was obviously enhanced in BNP-Tg mice, compared with non-Tg mice (Fig. 2*f*).

Angiogenesis Was Blunted in cGKI-Knockout Mice and Accelerated in cGKI-Tg Mice. The constitution of the homozygous mice gradually deteriorated and most of them died before 10 wk (15). Because nutrition may influence angiogenesis, we mainly compared heterozygous mutant mice ($cGKI^{+/-}$) with their control littermates ($cGK^{+/+}$). By LDPI analysis, limb perfusion among $cGKI^{+/-}$ mice remained significantly impaired throughout the 28-day follow-up period in comparison with $cGK^{+/+}$ (Fig. 3 *a* and *b*). In two cGKI-knockout mice ($cGKI^{-/-}$), recovery from limb ischemia was remarkably reduced, compared with $cGKI^{+/-}$ or $cGK^{+/+}$. Immunostaining of ischemic hindlimb tissue at day 28 with anti-PECAM-1 antibody revealed decreased capillary density in $cGKI^{+/-}$ (2,025 ± 51 per mm²) compared with $cGK^{+/+}$ (2,302 ± 87 per mm²; $P = 0.010$; Fig. 3 *c* and *d*). Two $cGKI^{-/-}$ mice had decreased capillary density (1,845 ± 163 per mm²) compared with $cGKI^{+/-}$ or $cGKI^{+/+}$.

By Northern blotting of cGKI-Tg mice, we confirmed overexpression of cGKI observed in the aorta and skeletal muscle compared with non-Tg mice (Fig. 3*e*). By immunostaining of cGKI, after antigen retrieval, high expression was also seen in the skeletal muscle and blood vessels (Fig. 3*f*). By LDPI analysis, cGKI-Tg mice showed significantly higher perfusion improvement at the end of the study compared with non-Tg mice (Fig. 3 *g* and *h*).

NPs Potentiated Capillary Network Formation of Cultured ECs. NPs significantly potentiated capillary network formation of human umbilical vein ECs in a bell-shaped fashion (Fig. 4 *a* and *b*). Network formation was prominent at 10^{-8} M ANP, 10^{-8} M BNP, and 10^{-10} M to 10^{-8} M CNP. The increase of network formation induced by NPs was completely blocked by Rp-8-pCPT-cGMP, a cGK inhibitor, at a concentration of 5×10^{-6} M (Fig. 4 *a* and *c*). Furthermore, treatment with 10^{-5} M PD 98059, an Erk1/2 inhibitor, significantly suppressed the increase of network formation induced by NPs (Fig. 4 *a* and *d*).

CNP Gene Transfer Enhanced Angiogenesis in Ischemic Hindlimb. CNP immunostaining was detected in skeletal muscle from the ischemic hindlimb of mice that received pAC.CMV/CNP at day 20 (Fig. 5*a*). Endogenous CNP was also detected in blood vessels of mice that received control vector, pAC.CMV (Fig. 5*a*; arrowhead). Plasma CNP level was similarly below sensitivity threshold value ($<1.32 \times 10^{-10}$ M) in mice injected with pAC.CMV/CNP or pAC.CMV. By LDPI analysis, mice receiving pAC.CMV/CNP showed a significant increase in blood flow at

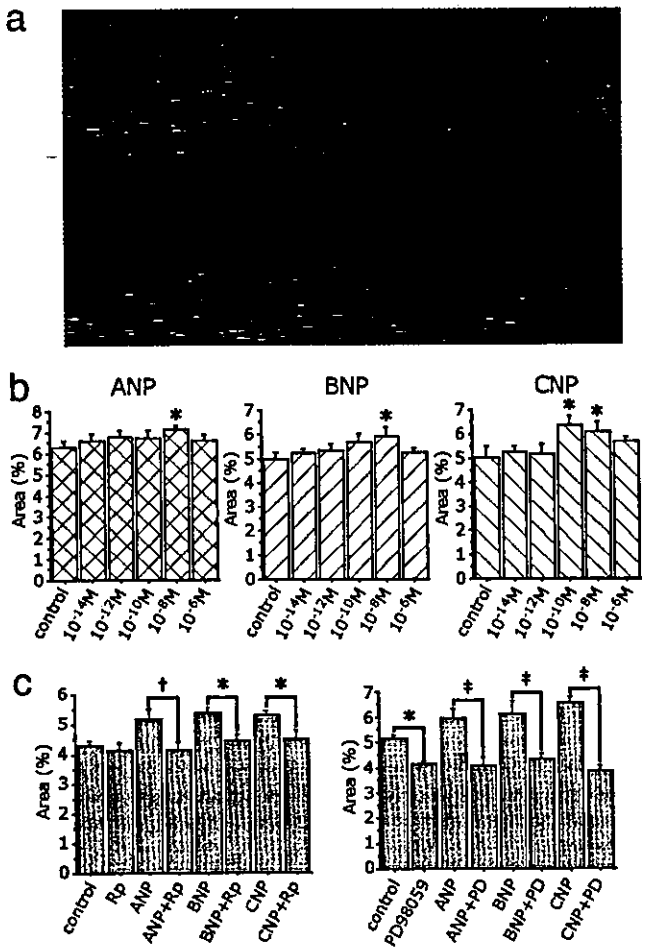

Fig. 4. NPs potentiated capillary network formation of cultured human umbilical vein ECs. (*a*) Capillary network formation by Matrigel assay in the presence of 10^{-8} M ANP, BNP, and CNP with or without Rp-8-pCPT-cGMP (Rp: 5×10^{-6} M), a cGK inhibitor, and PD 98059 (PD: 10^{-5} M), an Erk1/2 inhibitor. (*b*) Mean area of tube formation in the presence of various concentrations of ANP, BNP, and CNP. (*c* and *d*) Effects of Rp-8-pCPT-cGMP (*c*) and PD 98059 (*d*) in network formation induced by NPs. *, $P < 0.05$; †, $P < 0.01$; ‡, $P < 0.001$. (Scale bar, 500 μm.)

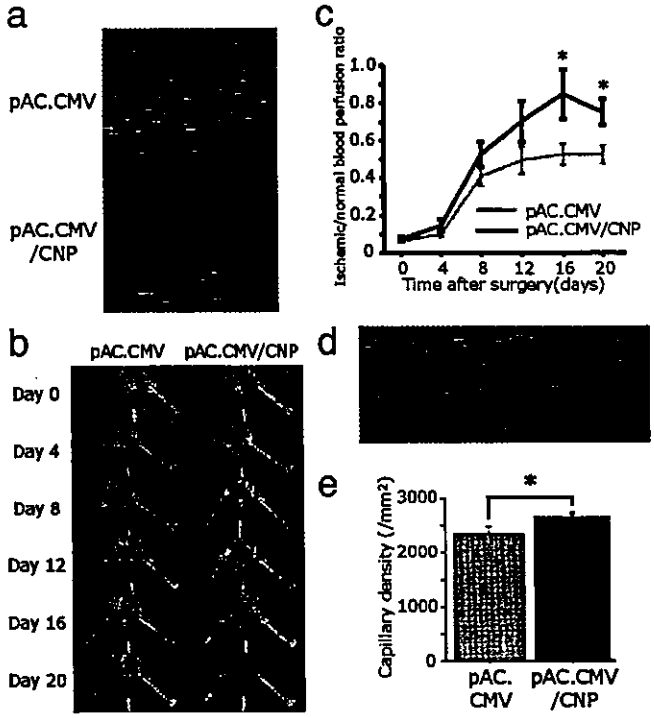

Fig. 5. Effect of CNP gene transfer in the murine ischemic hindlimb model. (*a*) CNP immunostaining (brown) after local injection of control vector (pAC.CMV) or pAC.CMV/CNP. (*b* and *c*) Serial LDPI measurements in mice receiving pAC.CMV or pAC.CMV/CNP ($n = 16$ per group). (*d* and *e*) PECAM-1 staining (bright red) of the ischemic hindlimb tissues at day 20 in mice injected with pAC.CMV or pAC.CMV/CNP (*d*), and quantitative analysis of capillary density (*e*) ($n = 10$ per group). *, $P < 0.05$. (Scale bars, 100 μm.)

the end of the study compared with mice receiving pAC.CMV (Fig. 5 *b* and *c*). Immunostaining of ischemic hindlimb tissues at day 20 with anti-PECAM-1 antibody revealed an increased capillary density in mice injected with pAC.CMV/CNP (2,643 ± 88 per mm^2) compared with pAC.CMV (2,364 ± 104 per mm^2; $P = 0.048$; Fig. 5 *d* and *e*).

Discussion

Experiments performed in this study reveal actions of NPs on vascular regeneration in response to ischemia. BNP overproduced systemically in mice accelerated angiogenesis in the setting of tissue ischemia with activation of Erk1/2 in blood vessels. This evidence was confirmed by a combination of LDPI analysis and capillary density measurement. In addition, overproduction of BNP compensated for impaired neovascularization because of L-NAME treatment. We also succeeded in demonstrating that ischemia-induced angiogenesis is significantly potentiated in cGKI-Tg mice, but attenuated in cGK-knockout mice. Furthermore, CNP gene delivery in the ischemic hindlimb could significantly enhance angiogenesis. These results indicate that the NPs/NO/cGMP/cGK pathway is critical for neovascularization *in vivo*.

NPs stimulate two biologically active receptors, GC-A and GC-B. We and others have demonstrated that ANP and BNP show high affinity for GC-A, whereas CNP selectively binds to GC-B (24). We have already reported that BNP-Tg mice show skeletal phenotypes through activation of the CNP/GC-B pathway (16, 24). It is important to clarify, therefore, whether the effects of BNP in the hindlimb ischemia model of BNP-Tg mice are mediated through GC-A, GC-B, or both. By immunostaining of these receptors in the ischemic hindlimb of BNP-Tg mice, we confirmed that both GCs expressed in ECs and SMCs. Considering the finding that CNP also enhanced angiogenesis in our model, activation of GC-B is more likely in BNP-Tg mice; however, the analyses of GC-A-knockout mice (25), which we recently developed, would provide answers to that question.

To supplement these *in vivo* findings with genetically engineered mouse models, we performed several *in vitro* experiments. In cultured ECs, NPs significantly increased capillary network formation at the concentrations of 10^{-10} to 10^{-8} M, which were the same as the plasma BNP level in BNP-Tg mice (14, 16). Early studies, including our own report, have shown that NPs inhibit EC proliferation (26) and migration (27). The concentrations of NPs used in these reports are much higher than physiological (1, 2) and, thus, the EC growth inhibition by NPs seems to be a result of a pharmacological effect. We also confirmed that NP-induced capillary network formation was significantly blocked by Rp-8-pCPT-cGMP and PD98059, indicating the involvement of cGK and Erk1/2 in this phenomenon. Furthermore, we recently observed that ANP increases cultured EC proliferation and migration *in vitro* by activating the cGK and subsequent Akt/PKB and Erk1/2 pathways (28). These results indicate that NPs can act directly on ECs and potentiate endothelial regeneration.

To achieve recovery from tissue ischemia, not only ECs but also SMCs must migrate and proliferate to produce functionally mature vessels (29). Early studies, including our own report, have

shown that NPs inhibit cell growth of vascular SMCs (3). From these reports, it is anticipated that newly formed vessels of BNP-Tg mice in our model might represent immature capillaries without adequate mural cell coating. However, we confirmed that ECs possessed adhering mural cells, and the capillary structures were not different in BNP-Tg or non-Tg mice. Furthermore, the α SMA-positive capillary density in BNP-Tg mice was significantly increased compared with non-Tg mice. These results suggest that antiproliferative effects of NPs on SMCs may not play a role in angiogenesis.

Recently, the participation of inflammation in angiogenesis has been an area of focus. Arras *et al.* (30) reported monocyte activation with the production of cytokines and vessel proliferation might associate with angiogenesis in a rabbit hindlimb ischemia model. Izumi *et al.* (31) reported that infarct size after myocardial ischemia/reperfusion injury was smaller in mice lacking GC-A, accompanied with decreases in neutrophil infiltration. From these results, angiogenesis in our model could be explained in part by potential proinflammatory effects of NPs. However, we confirmed that the number of infiltrating leukocytes in the ischemic limb of BNP-Tg mice was similar or even lower than that of non-Tg mice. This finding indicates that possible proinflammatory effects of NPs do not play a role in angiogenesis.

Nitrates, which are clinically used to relieve coronary vasoconstriction, might be useful for the management of vascular obstructions because NPs and NO share the same intracellular signal-transduction pathway. However, there is growing evidence that nitroglycerin-induced production of oxygen-derived free radicals such as superoxide plays an important role in mediating the tolerance and endothelial dysfunction in response to long-term treatment (32). However, the present study revealed that NPs suppress reactive oxygen production in inflammatory cells and blood vessels. Therefore, our findings suggest that NPs possess clinical advantages over nitrates.

The time course of vascular regeneration was different between BNP-Tg mice and cGKI-Tg/knockout mice. The changes in vascular regeneration in cGKI-Tg and cGKI-knockout mice were clearly opposite ("mirror image") and the continuous activation or inactivation of cGKI might result in the final augmentation or suppression of vascular regeneration, which indicates the significance of the cGKI activation level to determine the extent of vascular regeneration. On the other hand, no significant difference in the blood flow or capillary density was seen between BNP-Tg and non-Tg mice at the end of our study. Attenuation of overactivation of the cGMP/cGKI pathway can be one of the possible explanations; however, the expression of GC-A/GC-B showed no apparent difference between BNP-Tg and non-Tg mice at day 7, and also before ischemia (data not shown). Therefore, even if the attenuation of overactivation of cGKI might be the cause, it must not have occurred at the level of regulation of receptor expression.

Clinical applications of cardiovascular gene therapy have been launched during the last several years. However, we know very little about either the therapeutic or toxic effects of overexpressing angiogenic proteins, including VEGF. VEGF overexpression could accelerate atherosclerosis (33), promote pathological angiogenesis (34), or develop limb-threatening peripheral edema. Less adverse effects, such as edema, are seen in patients treated with ANP (35). We have demonstrated that NPs are the vasculoprotective factor against atherosclerotic lesion (4, 5). Furthermore, in the present study, we confirmed that angiogenesis was enhanced in hindlimb-ischemic mice after CNP gene transfer. From these results, NPs in clinical use seem to possess multiple coordinate actions that result in vascular protection and regeneration. In addition, inhibition of NPs can be a potential target of antineoplastic drugs for suppression of angiogenesis.

In conclusion, we have revealed an activity of the NPs/cGMP/cGKI pathway and suggest that NPs, as endogenous cardiovascular hormones, have significant advantages for the treatment of tissue ischemia. Thus, NPs can be used as a promising strategy for therapeutic angiogenesis in patients with tissue ischemia.

1. Sugawara, A., Nakao, K., Morii, N., Yamada, T., Itoh, H., Shiono, S., Saito, Y., Mukoyama, M., Arai, H., Nishimura, K., *et al.* (1988) *J. Clin. Invest.* **81,** 1962–1970.
2. Mukoyama, M., Nakao, K., Hosoda, K., Suga, S., Saito, Y., Ogawa, Y., Shirakami, G., Jougasaki, M., Obata, K., Yasue, H., *et al.* (1991) *J. Clin. Invest.* **87,** 1402–1412.
3. Komatsu, Y., Itoh, H., Suga, S., Ogawa, Y., Hama, N., Kishimoto, I., Nakagawa, O., Igaki, T., Doi, K., Yoshimasa, T. & Nakao, K. (1996) *Circ. Res.* **78,** 606–614.
4. Doi, K., Ikeda, T., Itoh, H., Ueyama, K., Hosoda, K., Ogawa, Y., Yamashita, J., Chun, T. H., Inoue, M., Masatsugu, K., *et al.* (2001) *Arterioscler. Thromb. Vasc. Biol.* **21,** 930–936.
5. Ohno, N., Itoh, H., Ikeda, T., Ueyama, K., Yamahara, K., Doi, K., Yamashita, J., Inoue, M., Masatsugu, K., Sawada, N., *et al.* (2002) *Circulation* **105,** 1623–1626.
6. Gerber, H. P., McMurtrey, A., Kowalski, J., Yan, M., Keyt, B. A., Dixit, V. & Ferrara, N. (1998) *J. Biol. Chem.* **273,** 30336–30343.
7. Fujio, Y. & Walsh, K. (1999) *J. Biol. Chem.* **274,** 16349–16354.
8. Fulton, D., Gratton, J. P., McCabe, T. J., Fontana, J., Fujio, Y., Walsh, K., Franke, T. F., Papapetropoulos, A. & Sessa, W. C. (1999) *Nature* **399,** 597–601.
9. Dimmeler, S., Fleming, I., Fisslthaler, B., Hermann, C., Busse, R. & Zeiher, A. M. (1999) *Nature* **399,** 601–605.
10. Ziche, M., Morbidelli, L., Choudhuri, R., Zhang, H. T., Donnini, S., Granger, H. J. & Bicknell, R. (1997) *J. Clin. Invest.* **99,** 2625–2634.
11. Hood, J. & Granger, H. J. (1998) *J. Biol. Chem.* **273,** 23504–23508.
12. Parenti, A., Morbidelli, L., Cui, X. L., Douglas, J. G., Hood, J. D., Granger, H. J., Ledda, F. & Ziche, M. (1998) *J. Biol. Chem.* **273,** 4220–4226.
13. Couffinhal, T., Silver, M., Zheng, L. P., Kearney, M., Witzenbichler, B. & Isner, J. M. (1998) *Am. J. Pathol.* **152,** 1667–1679.
14. Ogawa, Y., Itoh, H., Tamura, N., Suga, S., Yoshimasa, T., Uehira, M., Matsuda, S., Shiono, S., Nishimoto, H. & Nakao, K. (1994) *J. Clin. Invest.* **93,** 1911–1921.
15. Pfeifer, A., Klatt, P., Massberg, S., Ny, L., Sausbier, M., Hirneiss, C., Wang, G. X., Korth, M., Aszodi, A., Andersson, K. E., *et al.* (1998) *EMBO J.* **17,** 3045–3051.
16. Suda, M., Ogawa, Y., Tanaka, K., Tamura, N., Yasoda, A., Takigawa, T., Uehira, M., Nishimoto, H., Itoh, H., Saito, Y., *et al.* (1998) *Proc. Natl. Acad. Sci. USA* **95,** 2337–2342.
17. Elhage, R., Bayard, F., Richard, V., Holvoet, P., Duverger, N., Fievet, C. & Arnal, J. F. (1997) *Circulation* **96,** 3048–3052.
18. Tamura, N., Itoh, H., Ogawa, Y., Nakagawa, O., Harada, M., Chun, T. H., Suga, S., Yoshimasa, T. & Nakao, K. (1996) *Hypertension* **27,** 552–557.
19. Niwa, H., Yamamura, K. & Miyazaki, J. (1991) *Gene* **108,** 193–199.
20. Potter, L. R. & Garbers, D. L. (1992) *J. Biol. Chem.* **267,** 14531–14534.
21. Naruko, T., Ueda, M., van der Wal, A. C., van der Loos, C. M., Itoh, H., Nakao, K. & Becker, A. E. (1996) *Circulation* **94,** 3103–3108.
22. Miller, F. J., Jr., Gutterman, D. D., Rios, C. D., Heistad, D. D. & Davidson, B. L. (1998) *Circ. Res.* **82,** 1298–1305.
23. Toyokuni, S., Miyake, N., Hiai, H., Hagiwara, M., Kawakishi, S., Osawa, T. & Uchida, K. (1995) *FEBS Lett.* **359,** 189–191.
24. Chusho, H., Tamura, N., Ogawa, Y., Yasoda, A., Suda, M., Miyazawa, T., Nakamura, K., Nakao, K., Kurihara, T., Komatsu, Y., *et al.* (2001) *Proc. Natl. Acad. Sci. USA* **98,** 4016–4021.
25. Lopez, M. J., Wong, S. K., Kishimoto, I., Dubois, S., Mach, V., Friesen, J., Garbers, D. L. & Beuve, A. (1995) *Nature* **378,** 65–68.
26. Itoh, H., Pratt, R. E., Ohno, M. & Dzau, V. J. (1992) *Hypertension* **19,** 758–761.
27. Ikeda, M., Kohno, M. & Takeda, T. (1995) *Hypertension* **26,** 401–405.
28. Kook, H., Itoh, H., Choi, B. S., Sawada, N., Doi, K., Hwang, T. J., Kim, K. K., Arai, H., Baik, Y. H. & Nakao, K. (2003) *Am. J. Physiol.*, in press.
29. Folkman, J. (1982) *Ann. N.Y. Acad. Sci.* **401,** 212–227.
30. Arras, M., Ito, W. D., Scholz, D., Winkler, B., Schaper, J. & Schaper, W. (1998) *J. Clin. Invest.* **101,** 40–50.
31. Izumi, T., Saito, Y., Kishimoto, I., Harada, M., Kuwahara, K., Hamanaka, I., Takahashi, N., Kawakami, R., Li, Y., Takemura, G., *et al.* (2001) *J. Clin. Invest.* **108,** 203–213.
32. Sage, P. R., de la Lande, I. S., Stafford, I., Bennett, C. L., Phillipov, G., Stubberfield, J. & Horowitz, J. D. (2000) *Circulation* **102,** 2810–2815.
33. Inoue, M., Itoh, H., Ueda, M., Naruko, T., Kojima, A., Komatsu, R., Doi, K., Ogawa, Y., Tamura, N., Takaya, K., *et al.* (1998) *Circulation* **98,** 2108–2116.
34. Tanaka, Y., Katoh, S., Hori, S., Miura, M. & Yamashita, H. (1997) *Lancet* **349,** 1520 (lett.).
35. Saito, Y., Nakao, K., Nishimura, K., Sugawara, A., Okumura, K., Obata, K., Sonoda, R., Ban, T., Yasue, H. & Imura, H. (1987) *Circulation* **76,** 115–124.

0013-7227/04/$15.00/0
Printed in U.S.A.

Endocrinology 145(2):951–958

doi: 10.1210/en.2003-0816

Androgen Contributes to Gender-Related Cardiac Hypertrophy and Fibrosis in Mice Lacking the Gene Encoding Guanylyl Cyclase-A

YUHAO LI, ICHIRO KISHIMOTO, YOSHIHIKO SAITO, MASAKI HARADA, KOICHIRO KUWAHARA, TAKEHIKO IZUMI, ICHIRO HAMANAKA, NOBUKI TAKAHASHI, RIKA KAWAKAMI, KEIJI TANIMOTO, YASUAKI NAKAGAWA, MICHIO NAKANISHI, YUICHIRO ADACHI, DAVID L. GARBERS, AKIYOSHI FUKAMIZU, AND KAZUWA NAKAO

Department of Medicine and Clinical Science (Y.L., I.K., Y.S., M.H., K.K., T.I., I.H., N.T., R.K., K.T., Y.N., M.N., Y.A., K.N.), Kyoto University Graduate School of Medicine, Kyoto 606-8501, Japan; Howard Hughes Medical Institute and Department of Pharmacology (D.L.G.), University of Texas, Southwestern Medical Center at Dallas, Dallas, Texas 75390; and Center for Tsukuba Advanced Research Alliance (A.F.), Institute of Applied Biochemistry, University of Tsukuba, Tsukuba, Ibaraki 305-8571, Japan

Myocardial hypertrophy and extended cardiac fibrosis are independent risk factors for congestive heart failure and sudden cardiac death. Before age 50, men are at greater risk for cardiovascular disease than age-matched women. In the current studies, we found that cardiac hypertrophy and fibrosis were significantly more pronounced in males compared with females of guanylyl cyclase-A knockout (GC-A KO) mice at 16 wk of age. These gender-related differences were not seen in wild-type mice. In the further studies, either castration (at 10 wk of age) or flutamide, an androgen receptor antagonist, markedly attenuated cardiac hypertrophy and fibrosis in male GC-A KO mice without blood pressure change. In contrast, ovariectomy (at 10 wk of age) had little effect. Also, chronic testosterone infusion increased cardiac mass and fibrosis in ovariectomized GC-A mice. None of the treatments affected cardiac mass or the extent of fibrosis in wild-type mice. Overexpression of mRNAs encoding atrial natriuretic peptide, brain natriuretic peptide, collagens I and III, TGF-β1, TGF-β3, angiotensinogen, and angiotensin converting enzyme in the ventricles of male GC-A KO mice was substantially decreased by castration. The gender differences were virtually abolished by targeted deletion of the angiotensin II type 1A receptor gene (AT1A). Neither castration nor testosterone administration induced any change in the cardiac phenotypes of double-KO mice for GC-A and AT1A. Thus, we suggest that androgens contribute to gender-related differences in cardiac hypertrophy and fibrosis by a mechanism involving AT1A receptors and GC-A. (*Endocrinology* 145: 951–958, 2004)

MYOCARDIAL HYPERTROPHY IS prevalent in a substantial portion of individuals with essential hypertension (1, 2), and it is recognized as an independent risk factor for congestive heart failure and sudden cardiac death (3). Extended cardiac fibrosis results in increased myocardial stiffness, causing ventricular dysfunction and, ultimately, heart failure (4). Significant gender-related differences in the cardiovascular system are now well documented, and before the age of 50, men are at greater risk for cardiovascular diseases than age-matched women (5–9). However, the precise mechanism underlying gender-related differences in cardiac diseases is not fully understood. The results of both *in vitro* and *in vivo* studies indicate that sex steroids play a key role in the development of cardiac structural abnormalities. Estrogen and androgen receptors are present in myocardial tissues (10–12). Estradiol has antiproliferative effects on cardiac fibroblasts (13) and vascular smooth-muscle cells (14, 15), whereas androgens increase proliferation of vascular smooth-muscle cells (16). Studies using sinoaortic denervation-induced cardiac hypertrophy in rats have also shown that testosterone facilitates hypertrophy but estradiol inhibits it (17). A less severe model of cardiac hypertrophy in rats (swimming- or hypertension-induced) failed to confirm the antiproliferative effect of estradiol (18). Moreover, not all males, whether human or experimental animal, develop gender-related cardiac abnormalities. Somjen and colleagues (15) reported a biphasic proliferative response for both estrogen and testosterone in vascular smooth muscle and endothelial cells. It, therefore, is unclear how gender-induced changes in cardiac structural pathology are made manifest.

Mice lacking guanylyl cyclase A (GC-A), a natriuretic peptide receptor, exhibit salt-resistant hypertension, myocardial hypertrophy and interstitial fibrosis, and sudden death (before the age of 6 months) (19–20). In the present study, we found that male GC-A knockout (KO) mice show more pronounced cardiac hypertrophy and fibrosis compared with female GC-A KO mice and that gender-related differences are not seen in wild-type (WT) mice. Additionally, we found that these gender-related differences are attenuated either by castration or flutamide, an androgen receptor (AR) antagonist, and abolished by genetic disruption of angiotensin

Abbreviations: ACE, Angiotensin converting enzyme; Agt, angiotensinogen; Ang, angiotensin; ANP, atrial natriuretic peptide; AR, androgen receptor; AT1A, Ang II type 1A; BNP, brain natriuretic peptide; BW, body weight; GC-A, guanylyl cyclase-A; HR, heart rate; KO, knockout; LVW, left ventricular weight; OVX, ovariectomy; SBP, systolic blood pressure; WT, wild-type.

Endocrinology is published monthly by The Endocrine Society (http://www.endo-society.org), the foremost professional society serving the endocrine community.

(Ang) II type 1A (AT1A) receptors in male GC-A KO mice. We propose that androgens contribute to gender-related differences in cardiac structure and that the AT1A receptor and GC-A are involved in a reciprocal fashion.

Materials and Methods

Animals and treatments

All experimental procedures were carried out in accordance with Kyoto University standards for animal care. GC-A KO mice were originally generated at the University of Texas, Southwestern Medical Center at Dallas and Howard Hughes Medical Institute. Mice were housed in groups of three to five per cage under climate-controlled conditions with a 12-h light/dark cycle and were provided with standard food (CRF-1; Oriental Yeast Co., Ltd, Tokyo, Japan) and water *ad libitum*. The WT (GC-A+/+, AT1A+/+), AT1A KO (GC-A+/+, AT1A−/−), GC-A KO (GC-A−/−, AT1A+/+), and double-KO (GC-A−/−, AT1A−/−) mice used in these experiments were generated from heterozygous (GC-A+/−, AT1A +/−) mice after crossing of single GC-A KO (19) and AT1A KO (21) mice. The genetic background of the original GC-A KO and AT1A KO mice was C57BL/6. Genotypes were determined before and verified after experimentation using PCR. Comparisons of age and body weight (BW) between the KO and WT mice were made among littermates. Also comparisons of age, body weight, and systolic blood pressure (SBP) between control and treated mice were performed.

Measurement of heart rate (HR) and SBP

HR and SBP were measured in conscious mice using a computerized tail-cuff method (Softron Co., Ltd., Tokyo, Japan) (19, 21). Briefly, mice were restrained in a pocket and warmed at 38 C. HR and SBP were measured at 1000–1400 h and calculated as the average of six sessions per day after mice were adapted to the apparatus for 5 d. The validity of this system has been established previously in our laboratory (22).

Measurement of left ventricular weight (LVW) and interstitial fibrosis

After animals were killed by cervical dislocation under anesthesia with ether at 16 wk of age, the hearts were dissected out, LVW was measured, and its ratio to BW (LVW/BW) was calculated and used as an index of ventricular hypertrophy. The left ventricles were then fixed in 10% formalin and prepared for routine histological examination. To determine the degree of collagen fiber accumulation, we randomly selected 20 fields in three individual sections and calculated the ratio of the areas of van Gieson-stained interstitial fibrosis to the total left ventricular area using image analysis software and a Zeiss KS400 system; perivascular fibrosis was excluded in the present study.

mRNA analysis

Total mRNA was prepared from the left ventricle using TRIzol (Life Technologies Inc., Rockville, MD). Expression of mRNAs encoding atrial natriuretic peptide (ANP), brain natriuretic peptide (BNP), collagens I and III, TGF-β1, TGF-β3, angiotensinogen (Agt), and Ang converting enzyme (ACE) was evaluated using quantitative RT-PCR in a 7700 sequence detector (ABI PRISM, Applied Biosystems, Foster City, CA). The oligonucleotide primers are shown in Table 1. Glyceraldehyde-3-phosphate dehydrogenase mRNA was also amplified with specific primers and probe (Applied Biosystems).

Experimental protocols

We first compared the gender-related differences in the phenotypes of 16-wk-old GC-A KO and WT mice (n = 7–9 per group). HR and SBP were measured, and LVW, LVW/BW, and left ventricular fibrosis were calculated, after which related mRNA expression was analyzed.

To evaluate the involvement of estrogen in gender-related differences, we compared the phenotypes of sham-operated and ovariectomized (OVX) mice (n = 7–9 per group). Under anesthesia with ether, the ovaries of 10-wk-old female mice were exteriorized, ligated, and removed *via* bilateral paralumbar incisions, which were then closed with sutures. In sham mice, the ovaries were exteriorized and replaced, and the incisions were closed. Six weeks later, HR and SBP were measured, and the animals were killed.

To investigate the effects of androgens, male mice at 10 wk of age (n = 7–9 per group) were castrated using the trans-scrotal approach. Sham castration consisted of exteriorizing and replacing the testes. As in females, 6 wk later, HR and SBP were measured, and the animals were killed.

To confirm the role of androgen, we ovariectomized female WT and GC-A KO mice (n = 6–7 per group) under anesthesia with ether at 10 wk of age and sc implanted a testosterone pellet (25.0 mg/pellet, 60-darelease, catalog item SA-151) or vehicle pellet (placebo for testosterone, catalog item SC-111) (Innovative Research of America, Sarasota, FL) between the shoulders. Six weeks later, the animals were killed after HR and SBP were measured.

We further confirmed the role of androgens by chronically blocking AR with flutamide (23–24). Flutamide (Sigma Chemical Co., St. Louis, MO; 8 mg/kg·d, dissolved in polyethylene glycol 300) was sc infused for 6 wk using an osmotic mini-pump (model 2002, Alza Corp., Mountain View, CA) at 10 wk of age in male animals (n = 7–9 per group). The mini-pumps were sc implanted under the mice were anesthetized with

TABLE 1. Primer and probe sequences for RT-PCR assays

mRNA	Probe	Primers[a]
ANP	TGTACAGTGCGGTGTCCAACACAGAT	*f*GCCATATTGGAGCAAATCCT
		*r*GCAGGTTCTTGAAATCCATCA
BNP	TGCAGAAGCTGCTGGAGCTGATAAGA	*f*CCAGTCTCCAGAGCAATTCAA
		*r*GCCATTTCCTCCGACTTTT
AT1A	CCGGAATTCAACGCTCCCCA	*f*GTTTGCGCTTTTCATTACGAGT
		*r*TCTTGGTTAGGCCCAGTCCT
ACE	CACATCCCAAACGTGACACCGTACAT	*f*CGGAATGAAACCCATTTTGA
		*r*GCACAAAGCTCACGAAGTACC
Agt	AGGTTCTCAATAGCATCCTCCTCGAACTC	*f*CATTGGTGACACCAACCCC
		*r*GCTGTTCCTCCTCTCCTGCT
TGF-β1	AGCGCATCGAAGCCATCCG	*f*GACGTCACTGGAGTTGTACGG
		*r*GCTGAATCGAAAGCCCTGT
TGF-β3	CGGATGAGCACATAGCCAAGCA	*f*TTGAGCTCTTCCAGATACTTCG
		*r*TTCTTGCCACCTATGTAGCG
Collagen I	CACGGCTGTGTGCGATGACG	*f*GTCCCAACCCCCAAAGAC
		*r*CATCTTCTGAGTTTGGTGATACGT
Collagen III	TCCCACTCTTATTTTGGCACAGCAGTC	*f*TGGTTTCTTCTCACCCTTCTTC
		*r*TGCATCCCAATTCATCTACGT

Sequences are listed 5′ to 3′.

[a] Forward primers are designated by *f* and reverse primers by *r*.

ether and changed with new ones every 2 wk. Control mice were administered only vehicle. Six weeks later, the animals were analyzed.

To assess the involvement of the AT1A receptors in GC-A disruption-induced gender difference, we deleted AT1A receptor by the described method above. At 16 wk of age, the animals (n = 5–9 per group) were analyzed.

To further support the conclusion of AT1A receptor involvement, we castrated male double-KO mice (10 wk old; n = 5–6 per group) and chronically infused exogenous testosterone and analyzed the animals by the described methods above.

Statistical analysis

All results are expressed as means ± SEM. Data were analyzed by one-facter ANOVA. If a statistically significant effect was found, the Newman-Keuls test was performed to isolate the difference between the groups. Values of $P < 0.05$ were considered statistically significant.

Results

GC-A deficiency induces gender-related cardiac differences

Targeted deletion of GC-A led to increased LVW/BW ratios in both male and female mice. However, the effect was greater in males (58% increase *vs.* 33% increase in females; Fig. 1A). In contrast, in WT mice, there was no difference in LVW/BW ratio in males *vs.* females (Fig. 1A). In addition, male GC-A KO mice, but not WT mice, exhibited higher levels of left ventricular fibrosis than did females (378% *vs.* 44%, respectively; Fig. 1, B and C). On the other hand, there was no gender-related difference in HR (WT female 599.6 ± 26.1 *vs.* male 619.0 ± 52.4 beats/min; GC-A KO female 574.5 ± 25.9 *vs.* male 571.3 ± 28.1 beats/min; n = 7–9 per group) or in SBP (WT female 118.4 ± 1.7 *vs.* male 113.2 ± 3.4 mm Hg; GC-A KO female 140.0 ± 3.4 *vs.* male 147.4 ± 2.2 mm Hg; n = 7–9 per group) in either genotype. Male mice weighed more than females, but there was no difference between genotypes [WT female 25.0 ± 0.9 *vs.* male 32.3 ± 1.6 g ($P < 0.05$); GC-A KO female 25.1 ± 0.8 *vs.* male 31.6 ± 1.9 g ($P < 0.05$); n = 7–9 per group].

OVX has little effect in the heart

To elucidate a possible mechanism by which GC-A could prevent gender-related difference in the heart, we first investigated the effects of estrogen depletion. OVX had no effect on HR (WT sham 599.6 ± 26.1 *vs.* OVX 590.4 ± 17.9 beats/min; GC-A KO sham 574.5 ± 25.9 *vs.* OVX 582.3 ± 14.1 beats/min; n = 7–9 per group), SBP (WT sham 118.4 ± 1.7 *vs.* OVX 112.0 ± 2.2 mm Hg; GC-A KO sham 140.6 ± 3.4 *vs.* OVX 137.7 ± 3.0 mm Hg; n = 7–9 per group), LVW/BW ratio, ventricular fibrosis in either mouse type (Fig. 1, A–C), or BW (WT sham 25.0 ± 0.9 *vs.* OVX 25.6 ± 0.8 g; GC-A KO sham 25.1 ± 0.8 *vs.* OVX 25.1 ± 1.6 g; n = 7–9 per group).

Neither castration nor administration of an AR antagonist diminishes cardiac hypertrophy and fibrosis in male GC-A KO mice, whereas testosterone infusion increases cardiac hypertrophy and fibrosis in OVX GC-A mice

In contrast to OVX, removal of testes was associated with a marked reduction in the LVW/BW ratio and in ventricular fibrosis in GC-A KO mice (by 20.5 and 44.7%, respectively) but not to levels comparable to those seen in WT mice. Castration had no effect in WT mice (Fig. 1). Castration reduced BW in male WT as well as in male GC-A KO mice [WT 5.7 ± 0.5 *vs.* 2.1 ± 0.4 g ($P < 0.05$), and GC-A KO 6.6 ± 0.9 *vs.* 2.7 ± 0.6 g ($P < 0.05$) for sham and castrated groups, respectively; n = 7–9 per group]. Castration had no effect on HR (WT 619.0 ± 52.4 *vs.* 606.2 ± 45.9 beats/min, and GC-A KO 571.3 ± 28.1 *vs.* 600.2 ± 13.2 beats/min, for sham and castrated groups, respectively; n = 7–9 per group) or SBP

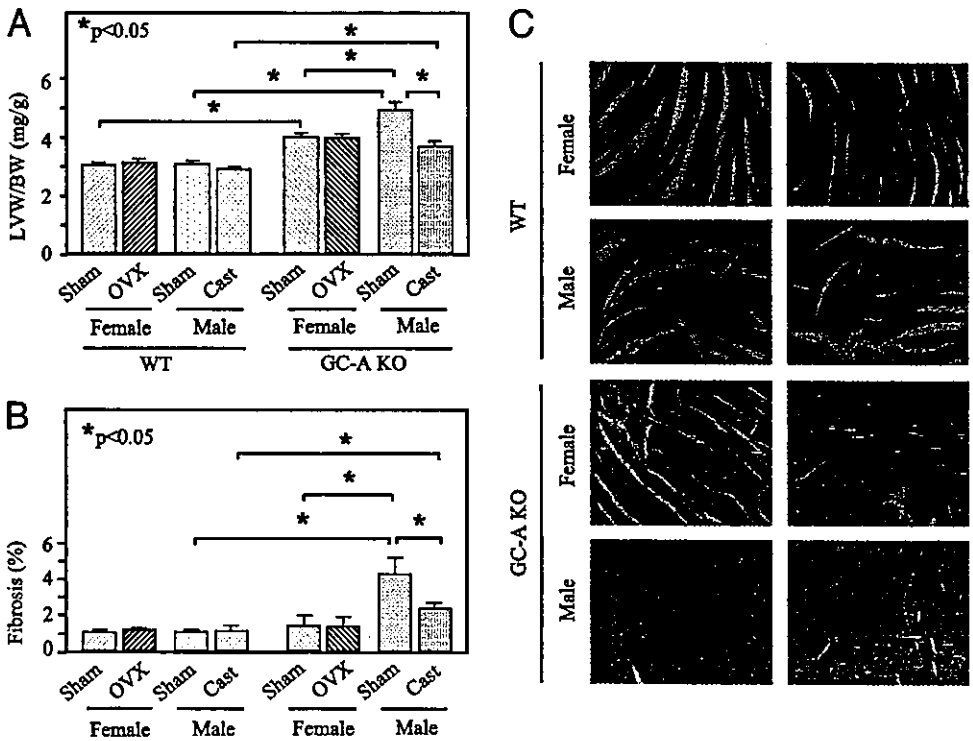

FIG. 1. GC-A disruption-induced gender-related differences in cardiac hypertrophy and fibrosis were inhibited by castration in male (Cast), but not in female (OVX) mice that were castrated at 10 wk and analyzed at 16 wk of age. The ratio of the areas of van Gieson-stained interstitial fibrosis to the total left ventricular area was calculated using image analysis software and a Zeiss KS400 system. A, LVW/BW ratio; B, relative levels of left ventricular fibrosis; C, photomicrographs showing representative examples of cardiac fibrosis (red) (magnification, ×200). Values are means ± SEM; n = 7–9 per group; *, $P < 0.05$.

(WT 113.2 ± 3.4 *vs.* 105.8 ± 4.2 mm Hg, and GC-A KO 147.4 ± 2.2 *vs.* 142.2 ± 6.3 mm Hg, for sham and castrated groups, respectively; n = 7–9 per group). The AR antagonist flutamide had similar effects to castration on LVW/BW, fibrosis (Fig. 2), HR (data not shown), and SBP (data not shown). In contrast, chronic infusion of testosterone increased LVW/BW ratio (by 20%) and cardiac fibrosis (by 114%) in OVX GC-A mice but not in OVX WT mice (Fig. 3). Testosterone treatment was also associated with increased BW in GC-A KO but not in WT mice]WT 2.6 ± 0.3 *vs.* 3.2 ± 0.3 g ($P < 0.05$), and GC-A KO 2.9 ± 0.2 *vs.* 5.2 ± 0.5 g ($P < 0.05$), for sham and testosterone-treated groups, respectively; n = 6–9 in each group[. HR and SBP were not affected by testosterone treatment (data not shown).

Gender-related difference in molecular expression profile

Basal left ventricular levels of ANP, BNP, collagen I, collagen III, TGF-β1, and TGF-β3 mRNAs were all higher in male than female GC-A KO mice. Castration of males decreased mRNA expression of these molecules to levels seen in females (Fig. 4). Again, no gender-related difference or castration-associated effects were seen in WT mice (Fig. 4). In contrast to the above mentioned genes, the levels of Agt and ACE mRNAs were higher in males than in females, and castration of males strongly suppressed their expression, and their levels were comparable in both genotypes of mice.

Deletion of AT1A abolishes gender-related cardiac differences

Deletion of the AT1A gene in GC-A KO mice reduced LVW/BW in both male and female mice, but the effects were more pronounced in the males (by 34 and 32.7% in males *vs.* 18 and 23.5% in females, respectively). AT1A deletion also markedly reduced cardiac fibrosis in male GC-A KO mice (by 57.5%). Gender-related cardiac differences (LVW/BW and fibrosis) were evident only in GC-A KO mice, but not in WT (as above), AT1A KO or double-KO mice (Fig. 5).

Castration or testosterone infusion fails to induce changes in cardiac mass and fibrosis in male double-KO mice

In contrast to the data obtained in GC-A KO mice (see above), neither castration nor testosterone infusion affected cardiac mass or the level of fibrosis in male double-KO mice (data not shown). Similarly, HR and SBP were unaffected by either castration or testosterone replacement (data not shown).

Discussion

As previous literatures documented significant gender-related differences in cardiovascular function and geometry (6, 7), the present study demonstrates that male GC-A KO mice show more marked left ventricular hypertrophy and severe interstitial fibrosis than female ones. Considering the protective effects of estrogen on the cardiovascular system (25, 26), we first investigated the effects of estrogens on the gender-related difference in the GC-A KO mouse hearts. Although OVX had little effect on cardiac mass and fibrosis in both WT and GC-A KO mice, there are still some possibilities that have not been addressed, such as, first, the fact that the effects of estrogen deprivation in women are not immediate; they develop over years, meaning that the 6-wk period of estrogen deprivation may be insufficient. Second, phytoestrogens are found in over 300 plants, including some used in human and animal diets (27–29). They can bind to the estrogen receptor and induce estrogen-like effects in animals, humans, and cells in culture. In the present study, we cannot exclude the possibility that the chow of mice may contain phytoestrogens, which may protect from (or limit) the effects of OVX. Therefore, the role of estrogen in gender-related cardiac difference observed in GC-A KO mice should be further clarified.

Next, we examined the effects of androgens. ARs are widely distributed in the cardiovascular system, where they have been identified on aortic, peripheral vascular, ventricular, and atrial myocytes (30), and were recently shown to mediate robust, testosterone-induced hypertrophic responses in cardiac myocytes (12). Nevertheless, although virtually all men have much higher levels of androgens than women do, not all men exhibit more severe cardiac hypertrophy and fibrosis. In the present study, significant gender-related differences in cardiac abnormalities were observed only in GC-A KO mice. In addition, it is notable that both castration and AR antagonist markedly diminished cardiac hypertrophy and fibrosis in male GC-A KO mice, and chronic

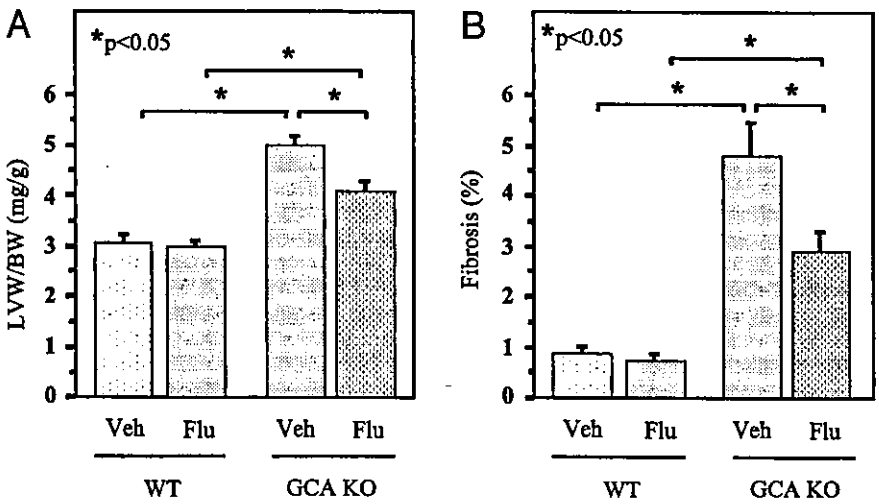

FIG. 2. Chronic AR blockade with flutamide was associated with decreased LVW/BW (A) and left ventricular fibrosis (B) in male GC-A KO mice. Flutamide (Flu; 8 mg/kg·d) or vehicle (Veh) was sc infused for 6 wk starting at 10 wk of age. Values are mean ± SEM; n = 7–9 per group; *, $P < 0.05$.

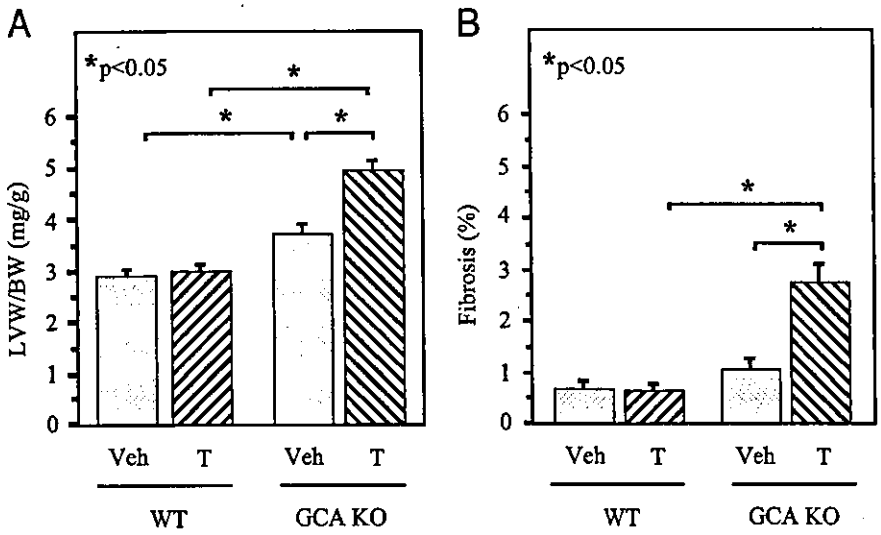

FIG. 3. Chronic infusion of testosterone (T) was associated with an increased LVW/BW (A) and left ventricular fibrosis (B) in OVX GC-A KO but not in OVX WT mice. A testosterone pellet (25.0 mg/pellet) or vehicle (Veh) was implanted sc at 10 wk of age, and 6 wk later, the animals were killed and analyses performed. Values are mean ± SEM; n = 6–7 per group; *, $P < 0.05$.

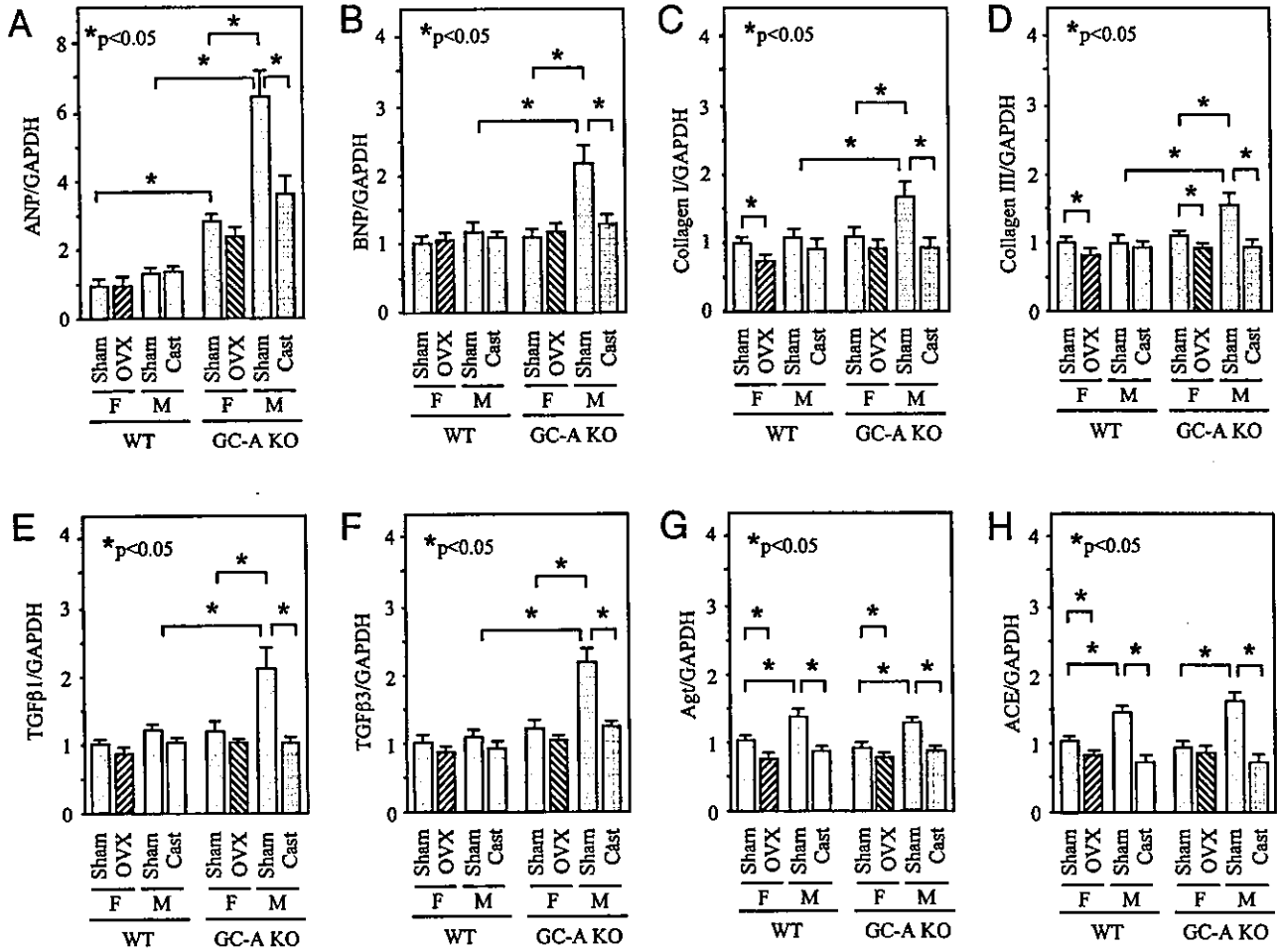

FIG. 4. Left ventricular levels of ANP, BNP, collagen I, collagen III, TGF-β1, and TGF-β3 mRNAs were elevated in male (M) GC-A KO mice and were reduced by castration to levels seen in females (F). Enhanced levels of Agt and ACE expression in male WT and GC-A KO mice were suppressed by castration, and levels were comparable in both genotypes. mRNAs were evaluated using quantitative RT-PCR in a 7700 sequence detector (ABI PRISM). Levels in sham female WT mice were arbitrarily assigned a value of 1.0. A, ANP; B, BNP; C, collagen I; D, collagen III; E, TGF-β1; F, TGF-β3; G, Agt; H, ACE. Values are mean ± SEM; n = 7–9; *, $P < 0.05$.

testosterone infusion increased cardiac mass and fibrosis only in OVX GC-A KO mice. ANP and BNP are well established molecular markers for cardiac hypertrophy. It has been demonstrated that the testosterone metabolite dihydrotestosterone is able to increase ANP secretion from ventricular myocytes. An AR antagonist, cyproterone, abolished